Pergamon

0148-9062(95)00078-X

Int. J. Rock Mech. Min. Sci. & Geomech. Abstr. Vol. 33, No. 5, pp. 513–537, 1996

0148-9062/96 $15.00 + 0.00

Evaluation of Safety Factors in Discontinuous Rock

E. ALONSO†
I. CAROL†
C. DELAHAYE‡
A. GENS†
P. PRAT†

Safety factors for kinematically admissible failure mechanisms in jointed rock masses have been defined with linear and nonlinear failure criteria for rock discontinuities. Data required to compute these safety factors are obtained by means of two finite element analyses of the effects of selfweight and external (structural) loading, respectively. Both types of analysis are closely linked since they share a common geometry. Joint elements are used to simulate the behaviour of rock discontinuities. If kinematically admissible mechanisms are possible under field conditions, the finite element mesh should also allow them to develop. Different aspects of the methodology have been illustrated through the safety evaluation of a 150 m high arch dam and its foundation in fractured cretaceous limestone. Special attention has been paid to the modelling of a realistic geometry including three-dimensional rock blocks and discontinuities. The paper discusses the effect of initial state of stress, the evolution of safety as the external load increases and the relation between the defined safety factors. It also provides practical guidelines for conducting this type of analysis in complex situations. Copyright © 1996 Elsevier Science Ltd.

INTRODUCTION

Safety analysis in engineering practice is often linked to simple definitions such as safety margin or safety factor. These factors try to provide a "distance" between the service or "as built" conditions and the failure state. Failure states are, however, difficult to define in complex cases and the classical definitions of safety are open to criticisms because of their inconsistency and poor overall representation of risk interpreted in a probabilistic sense. However, simple definitions of safety, amenable to calculation in real cases continue to provide a useful tool for designers. Safety factors are usually interpreted within the framework of an accepted scale for which there exists some previous experience.

A particularly complex case is the safety analysis of arch dams founded on fractured rock. A traditional way to investigate the behaviour of these structures has been to conduct model tests in which the dam is brought to failure by a progressive increase of the loads that simulate the hydrostatic load on the structure.

However, 1-g models do not satisfy conditions between model and prototype, as the failure criteria for joints and rock masses depend (in a nonlinear way) on the state of stresses. These type of models represent only a qualitative approximation to the problem. Centrifuge testing offers a theoretically better alternative, but its cost and practical limitations have to be compared with the possibilities offered by numerical techniques.

Modern numerical techniques to investigate the behaviour of rock masses include finite elements and distinct element methods (FEM and DEM). As pointed out in a recent review by Hart [1], DEM techniques are specifically suited to carry out discontinuum analyses in rock, but suffer some practical limitations, particularly in static problems, since stability and convergence depend on the proper selection of a time step and damping parameters (where the user making selection may have limited information of the system performance). Both FE methods (in which discontinuities are modelled by joint elements) and DEM techniques share major difficulties when they are confronted with the need to represent in a consistent way the internal geometry of the rock mass in real problems. In fact, the model geometry, which cannot be expected to

†E.T.S., Ingenieros de Caminos, UPC, Barcelona, Spain.
‡Universidad Nacional de San Juan, Argentina.

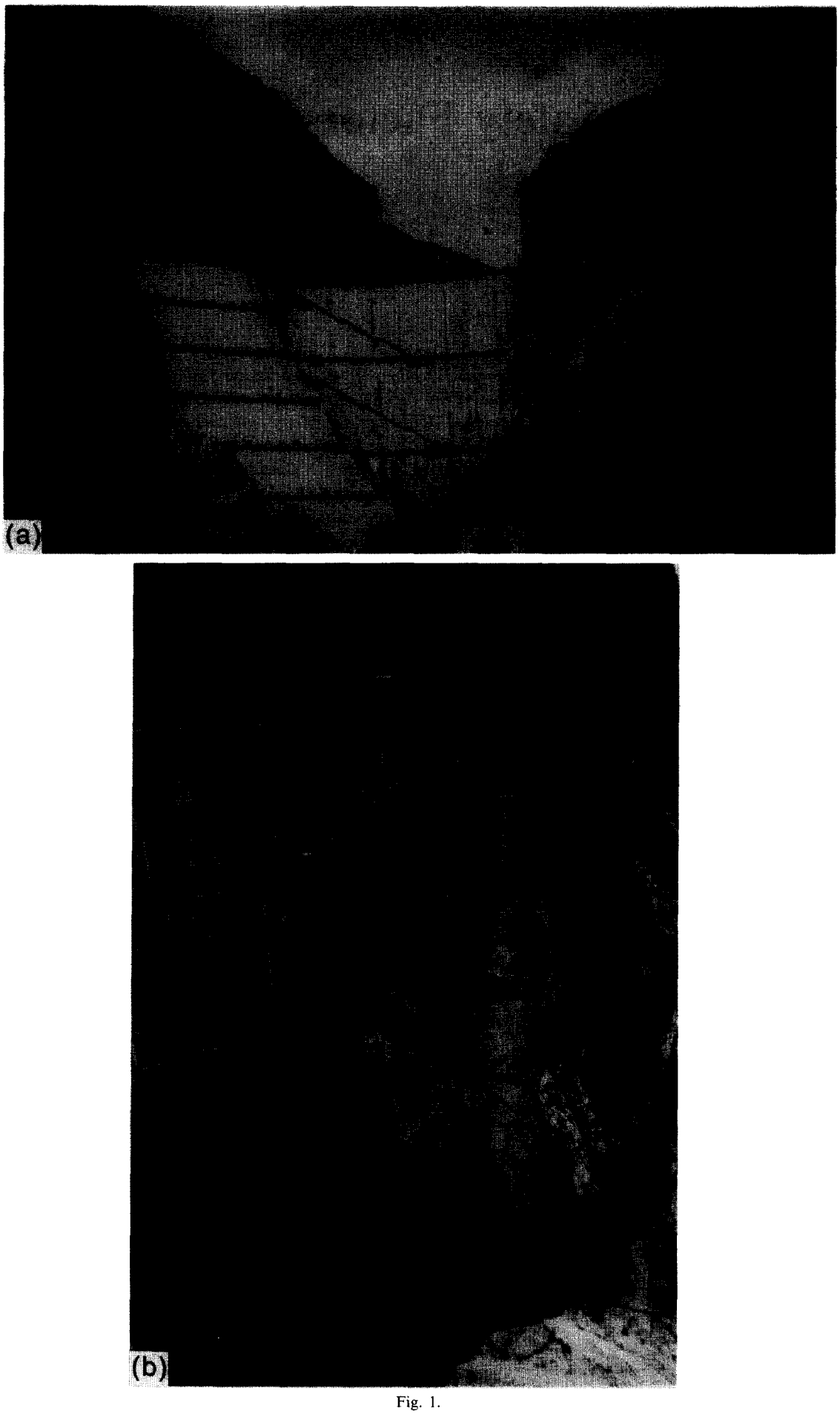

Fig. 1.

reproduce the real case, must at least be able to accommodate the most significant failure mechanisms that may eventually develop under external loading. There are no detailed rules to reduce real geometry into a representative simplified model, and, a compromise that takes into account the available computer and human resources, as well as the capability of the numerical codes, has to be reached. In this context, it is probably wiser to reduce the complexity of the constitutive models adopted for joint behaviour and to improve the geometrical characterization of the rock to reduce the risk of excluding a dominant failure mechanism.

Even if an appropriate representation of the rock structure is achieved using, for instance, solid and joint elements in a FE type of analysis, it is necessary to relate the stress–strain-displacement information resulting from the numerical analysis with a safety measure such as the safety factor. This is the problem discussed in this

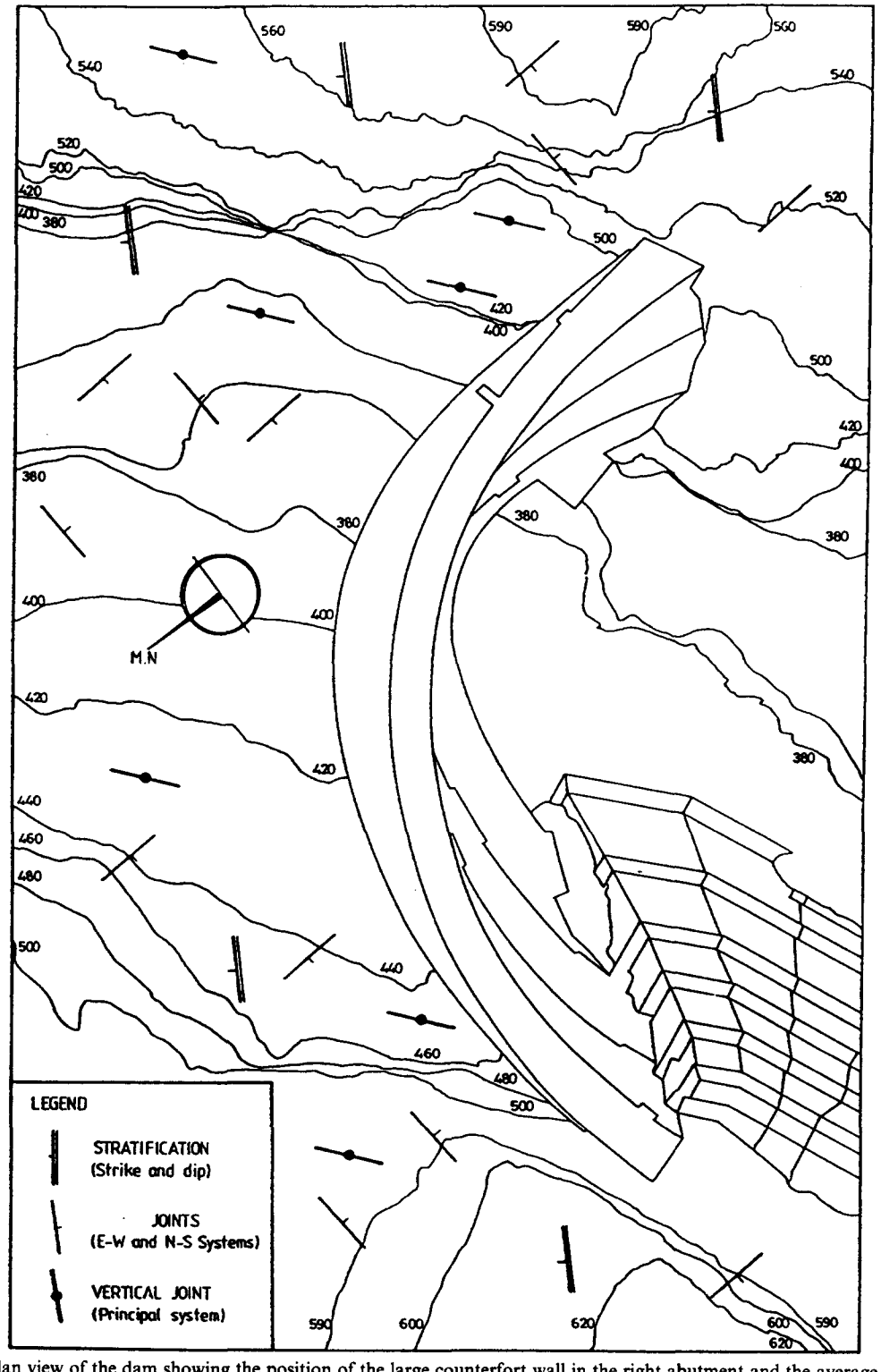

Fig. 2. Plan view of the dam showing the position of the large counterfort wall in the right abutment and the average fracture pattern of the rock mass at both abutments.

paper. In order to do so, alternative definitions of safety factor will be given in the next section and procedures to compute them, once a numerical analysis has been performed, will also be given. In addition, the proposed methodology will be applied to an interesting case: the safety conditions of a large arch dam: Canelles dam located in the Noguera Ribagorzana river, Catalunya, Spain, which was completed in April 1958. Aspects of the design, construction and subsequent remedial works carried out in this dam have been reported in several papers [2–4].

Canelles dam is a 151 m high arch structure founded on cretaceous massive limestone that is fractured by a main set of vertical joints (principal system) parallel to the valley (Fig. 1). In addition, bedding planes dip 45° upstream. Figure 2 shows a plan view of the dam with an indication of the strike and dip orientation of main joints observed. A large stabilizing counterfort wall anchored to the rock was built downstream of the right abutment in the place of a depression of the valley slope (Figs 1 and 2).

The dam was placed at the end of a steep canyon with apparently little rock mass to provide passive support to the arch loads. In addition, the unfavourable orientation of the principal system of joints (parallel to the canyon) has given rise to some concern about the stability of the dam and its foundation ever since its completion in 1958.

In a plane strain 2D analysis of the dam foundation carried out by Alonso and Carol [5] it was concluded that the safety factor against sliding of critical wedges was critically dependent on the average normal stress of joints of the principal system. The intensity of the initial normal stress required to ensure equilibrium of critical wedges has been plotted across the height of the dam in Fig. 3. There was, however, no reliable basis to estimate the actual distribution of initial stresses in the rock. In addition, the question of the important 3D effects of the problem remained unanswered, and therefore the safety conditions of the dam remained essentially unknown.

More recently, however, a continuing effort has been directed towards developing a better understanding of the safety conditions of the dam. The cretaceous rock foundation was investigated by means of a detailed reconnaissance program that included the performance of numerous large scale *in situ* shear tests on main rock discontinuities. Data gathered have been incorporated into the safety analysis described in this paper.

SAFETY OF STRUCTURES FOUNDED ON FRACTURED ROCK

In order to provide a quantitative assessment of the degree of safety of the dam/foundation ensemble it is useful to define a global safety measure that can be ascribed to potential failure mechanisms. In this way, the most critical mechanisms can be objectively identified.

Two alternative definitions of safety factor, λ_E and λ_ϕ, will be employed in this paper. λ_E is defined as the ratio between the maximum external load which is able to induce the sliding instability of a portion of jointed rock

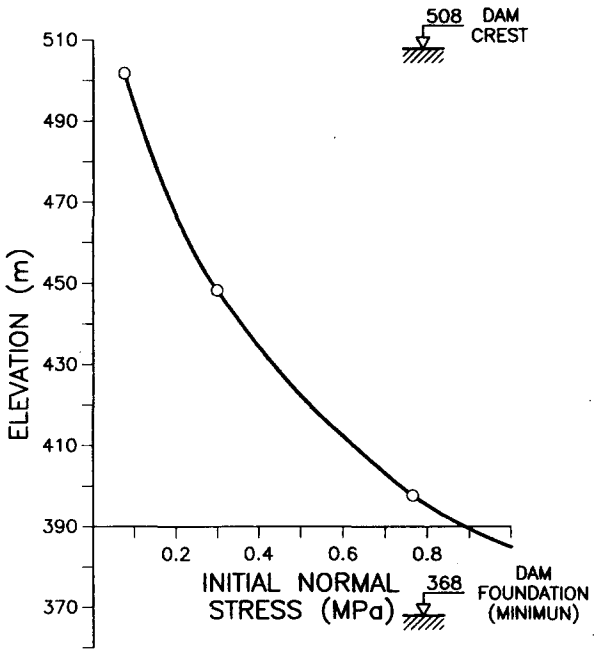

Fig. 3. Distribution of initial normal stress necessary for equilibrium. Two dimensional analysis.

mass and the actual load applied to the structure. In the case of dams founded on rock, the external load considered is the hydrostatic load (over the dam itself and the impervious curtains). λ_E is therefore a multiplying factor of the hydrostatic load. It may be regarded as unrealistic since it is difficult to think of actual circumstances which are capable of increasing hydrostatic load over the maximum ones foreseen in the project. In other words, in a case such as a dam, the maximum hydrostatic loads is not a particularly uncertain factor. λ_E retains, however, its character as a measure of the safety of the structure since it gives an indication of its capability to withstand external loads. This is also the sense of the usual definition of safety factor in foundation problems as the ratio between the load inducing failure and the actually applied load. Note that in our case a λ_E safety factor will be found for each admissible sliding mechanism within the jointed rock which may be brought to failure by increasing the external load. If one considers all the possible mechanisms, the minimum of λ_E values could be regarded as the safety factor of the structure.

λ_ϕ does not imply any increase in external loads. For a given potentially unstable sliding mechanism within the rock mass, λ_ϕ is the ratio between the shear strength of joints bounding the mechanism and the average shear stress required for equilibrium under the applied external loads. This definition is closely related to the concept of uncertainty in the actual values of rock joint strength parameters. Compared with λ_E, λ_ϕ may be regarded as a more realistic measure of safety since there are important reasons (rock variability, experimental difficulties) to make uncertain the shear strength of a rock joint. Again in this case a λ_ϕ factor may be found for each potentially unstable mechanism. The minimum over the set of unstable mechanisms may be considered as the λ_ϕ safety

factor of the structure. λ_ϕ is equivalent to the definition of safety usually found in limit equilibrium methods in connection, for instance, with slope stability problems.

The condition of stability of a portion of the rock mass bounded by discontinuities is used in the definition of both λ_E and λ_ϕ. The onset of instability is defined in terms of static equilibrium of forces along a particular direction of sliding. These two factors will now be derived in explicit form.

Failure against increase in external loads [Failure load] (λ_E)

To derive λ_E the external loads are separated into dead loads, $\boldsymbol{G}$, which remain constant and the active loads, $\boldsymbol{E}$, which may increase to failure. In this case, the dead loads are those due to gravity (self-weight), and the active loads are those due to the hydrostatic pressure acting on dam and grout curtain.

It can be argued that this distinction is adapted to a particular type of problem (arch dam under hydrostatic "external" loads). In other cases, alternatives that reflect the analyst's opinion regarding the type of external actions, their expected magnitude, variation or probability of occurrence are also possible.

A certain failure surface, S (see illustrative sketch in Fig. 4a) fully composed of joint elements is now considered together with a sliding direction defined by the unit vector $\boldsymbol{d}$. S defines a rock wedge acted, in general, by external active as well as gravity forces. The resultants of those forces on the considered rock mass are the vector $\boldsymbol{G}$ (gravity force) and $\boldsymbol{E}$ (active external load). If the rock wedge reaches boundary of the discretized mesh where displacement conditions are imposed (fixed nodes, for instance) some boundary reactions $\boldsymbol{R}_G$ and $\boldsymbol{R}_E$ will also act on the rock wedge (Fig. 4b,c). From the finite element analysis, the stresses on the failure surface are known for both the gravity forces, $\boldsymbol{\sigma}_G = (\sigma_G, \tau_G)$, and the active loads $\boldsymbol{\sigma}_E = (\sigma_E, \tau_E)$. σ and τ denote, respectively, normal and shear stresses on the joints.

When the rock wedge moves along the $\boldsymbol{d}$ direction, the two sides of every boundary joint either slide one against the other or they separate so that the joint is open. The case of penetration would indicate a kinematically incompatible movement and a new direction $\boldsymbol{d}$ should be chosen. Equilibrium will be established at the beginning of the motion and therefore only the portions of the boundary surface actually sliding (and not opening) will be considered. This portion will be denoted as S_1. In the sketch of Fig. 4 for the horizontal motion defined by $\boldsymbol{d}$ the vertical portion *ab* of the joint will open and only the base joint *bc* will slide. For this case S_1 is simply the segment *bc*.

When the external active loads reach a value $\lambda_E\ \boldsymbol{E}$ (motion starts) the surface S_1 will have reached its limiting condition given by the shear strength τ^{max}. Note also that stresses τ^{max} act in the direction of $\boldsymbol{d}$. Static equilibrium of forces along direction $\boldsymbol{d}$ acting on the rock

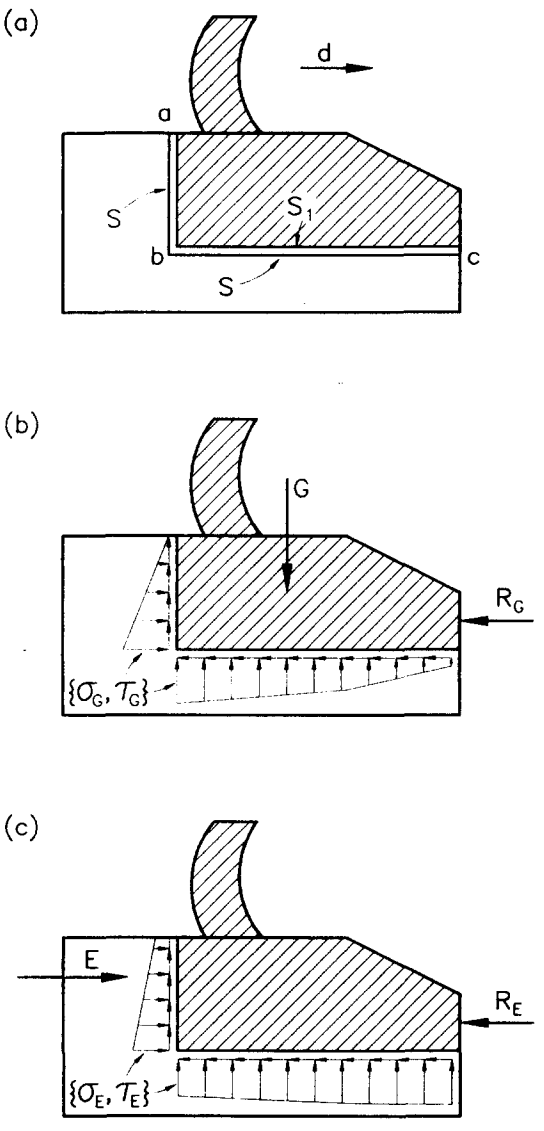

Fig. 4. (a) Failure surface. Load and stresses; (b) Self-weight; (c) Hydrostatic pressure.

wedge at that particular instant can be written as follows:

$$\boldsymbol{d}^t[(\boldsymbol{G} + \boldsymbol{R}_G) + \lambda_E(\boldsymbol{E} + \boldsymbol{R}_E)] = \int_{S_1} \tau^{max} ds. \qquad (1)$$

The vector products indicated in the left hand side are internal (scalar) products.

Linear Mohr–Coulomb strength envelope. In this case τ^{max} is given by

$$\tau^{max} = c + \sigma \tan \phi. \qquad (2)$$

Equation (1) was established for the external load, $\boldsymbol{G} + \lambda_E\ \boldsymbol{E}$, acting on the rock wedge. Therefore, in order to substitute equation (2) into (1) the normal stress on the joints, σ, should correspond to that particular loading. It will be assumed that the normal stresses due to $\boldsymbol{E}$ increase in the same proportion as $\boldsymbol{E}$ increases. Therefore

$$\sigma = \sigma_G + \lambda_E \sigma_E. \qquad (3)$$

Substitution of equation (2) into (1) taking into account equation (3) leads to the following explicit expression for λ_E:

$$\lambda_E = \frac{C + N_G \tan\phi - \boldsymbol{d}^t(\boldsymbol{G} + \boldsymbol{R}_E)}{\boldsymbol{d}^t(\boldsymbol{E} + \boldsymbol{R}_E) - N_E \tan\phi} \tag{4}$$

where

$$N_G = \int_{S_1} \sigma_G \, ds, \; N_E = \int_{S_1} \sigma_E \, ds \text{ and } C = \int_{S_1} c \, ds.$$

If the potentially unstable rock block does not include any mesh node with prescribed motion, then

$$\lambda_E = \frac{C + N_G \tan\phi - \boldsymbol{d}^t\boldsymbol{G}}{\boldsymbol{d}^t\boldsymbol{E} - N_E \tan\phi}. \tag{5}$$

Note that in order to compute λ_E, the distribution of stresses along the limiting surfaces defining a potentially unstable block should be evaluated. They may be taken from a numerical analysis of the problem in which the effects of selfweight and external loads are specifically known. Once S and $\boldsymbol{d}$ are proposed the value of λ_E can be computed. Note that the fundamental assumption in this derivative is that normal stresses induced by increasing external loads increase in the same proportion (3). The accuracy of expression (4) or (5) depends therefore on the degree of fulfillment of this assumption.

Nonlinear strength envelope. Several nonlinear failure envelopes have been proposed over the past three decades in order to approximate the results of shear testing on rock joints. Carol *et al.* [6] proposed a two parameter hyperbolic envelope. They showed that this simple criteria which is expressed as

$$\tau^{\max} = \sqrt{\sigma \tan\phi (2c + \sigma \tan\phi)} \tag{6}$$

where ϕ is the limiting friction angle for high normal stresses and c is the cohesion intercept of hyperbola asymptote, fits published strength results as accurately as other well known failure criteria. When $c = 0$, expression (6) becomes the Mohr–Coulomb equation without cohesion. The elastoplastic explicit stress–strain model of joint behaviour in shear, adopted in the FE analysis performed, is derived in the Appendix. It uses the hyperbolic model as a yield criterion. If equation (6) is introduced into (1), and equation (3) is taken into account, the following implicit expression for λ_E is obtained

$$\boldsymbol{d}^t[(\boldsymbol{G} + \boldsymbol{R}_G) + \lambda_E(\boldsymbol{E} + \boldsymbol{R}_E)] = \int_{s_1} \sqrt{(\sigma_G + \lambda_E\sigma_E)\tan\phi\,[2c + (\sigma_G + \lambda_E\sigma_E)\tan\phi]}\,ds. \tag{7}$$

From this equation the value of the factor of safety λ_E can be obtained by iterations in which the integral over the portion of sliding surface S_1 must be computed.

Uncertainty in strength parameters (λ_ϕ)

The definition of λ_ϕ given before may be written as

$$\lambda_\phi = \frac{\tau^{\max}}{\tau^{\text{mob}}} \tag{8}$$

where τ^{mob} may be called the "mobilized" shear stress. It should be in equilibrium with the actual set of applied external loads acting on the potentially unstable rock block. This static equilibrium of forces, along direction $\boldsymbol{d}$, is expressed as

$$\boldsymbol{d}^t[(\boldsymbol{G} + \boldsymbol{R}_G) + (\boldsymbol{E} + \boldsymbol{R}_E)] = \int_{S_1} \tau^{\text{mob}} \, ds \tag{9}$$

where τ^{mob} acts in the direction of $\boldsymbol{d}$ only along the portion S_1 of the boundary surface for the reasons given previously. $\tau^{\max}$, the joint shear strength, corresponds now to the actual normal distribution of normal stresses acting on the boundary joints for the set of external loads $\boldsymbol{G} + \boldsymbol{E}$. They are computed by adding the contributions of the active load and gravitational load as obtained in the finite element analysis

$$\sigma = \sigma_G + \sigma_E. \tag{10}$$

Linear Mohr–Coulomb failure envelope. If τ^{mob} from equation (8) is substituted into equation (9), and equations (2) and (10) are taken into account, the following explicit expression is found for λ_ϕ

$$\lambda_\phi = \frac{C + \tan\phi(N_G + N_E)}{\boldsymbol{d}^t[(\boldsymbol{G} + \boldsymbol{R}_G) + (\boldsymbol{E} + \boldsymbol{R}_E)]} \tag{11}$$

where C, N_G, N_E have the same meaning as in equation (4).

If node reactions are not included in the rock block under consideration, equation (11) simplifies to

$$\lambda_\phi = \frac{C + \tan\phi(N_G + N_E)}{\boldsymbol{d}^t(\boldsymbol{G} + \boldsymbol{E})}. \tag{12}$$

Nonlinear hyperbolic failure envelope. If $\tau^{\max}$ from equation (6) is now considered instead of the Mohr–Coulomb criterion, equations (6), (8), (9) and (10) lead to the following expression for λ_ϕ

$$\lambda_\phi = \frac{\int_{s_1} \sqrt{(\sigma_G + \sigma_E)\tan\phi\,[2c + (\sigma_G + \sigma_E)\tan\phi]}\,ds}{\boldsymbol{d}^t[(\boldsymbol{G} + \boldsymbol{R}_G) + (\boldsymbol{E} + \boldsymbol{R}_E)]}. \tag{13}$$

Note that, unlike λ_E, the expression for λ_ϕ is always explicit irrespective of the nonlinearity of the failure criteria.

Any of the derived expressions for the safety factor [equations (4), (7), (11) or (13)] require:

(1) A stress analysis in which the effect of selfweight and external actions are successively identified.
(2) A specific failure surface together with a sliding direction should be selected. The distribution of normal stresses on the joints defining this failure surface is required to compute the surface integrals included in the expressions for λ_E and λ_ϕ. Only failure configurations which are a combination of the set of joints included in the finite element discretization can be possibly analyzed. Numerical analysis is therefore closely linked with the safety analysis and this relationship should be

taken into account when the geometrical discretization of the problem is carried out. Note also that safety factors may be derived from a purely elastic analysis or a full nonlinear analysis of the problem. Nonlinear analysis, carried out to the vicinity of failure (by increasing external load, for instance) offers, however, the possibility of rating the accuracy of safety factors as defined in the previous equations.

The proposed method will be applied to the evaluation of safety of Canelles dam but, before, an example of determination of λ_E and λ_ϕ for a very simple problem will be given.

Example. Consider in Fig. 5a a gravity dam, vertical face upstream, founded on a parallelepipedic rock block. The block has been isolated in Fig. 5b for better reference. A vertical grout curtain has been built from the upstream lower corner of the dam so that full hydrostatic load acts on the upstream face of the rock block ($B_1A_1C_1D_1$). No water pressure acts, however, on the two lateral vertical joints, ($A_1A_2C_2C_1$) and ($B_2B_1D_1D_2$), and on the lower horizontal joint ($C_1C_2D_2D_1$). The downstream face of the block ($A_2B_2D_2C_2$) is a vertical cliff so that a horizontal motion of the dam and the foundation block is a kinematically admissible global failure mechanism.

The failure surface S in this example is given by the two lateral joints, the base joint and the upstream joint. Upon application of a hydrostatic load (the height of water above foundation level is h_w) the upstream joint will tend to open and no shear stresses could be developed in that face. Therefore, the resisting surface, S_1, will be given by the lateral as well as the base joints. Dimensions of the foundation block are b (height), l (length) and e (thickness).

Consider in Fig. 6a a cross-section along the midplane of the block ($U_1U_2L_2L_1$) and a plan view. Also indicated are forces on the sliding block and stresses on the surface S_1 divided in two parts: those due to the gravity forces (Fig. 6b) and those due to the hydrostatic external loads (Fig. 6c). Concerning the normal stresses across the lateral joints a K_0 condition will be assumed whereby they will be computed as K_0 times the vertical stresses in the block derived from gravity forces. A cartesian coordinate system centred at point L_1 is chosen for reference (Figs 5b and 6a). The considered motion of the block is defined by the unit vector $\boldsymbol{d}\equiv(1, 0, 0)'$.

The following gravity forces are considered: the weight of the dam $\boldsymbol{W}_d = W_d\,(0, 0, 1)'$ and the rock weight $\boldsymbol{W}_r = W_r\,(0, 0, 1)'$, where W_d and W_r are the weight intensities. Rock is assumed to have a constant unit weight, γ_r. It will be assumed that due to the high stiffness of joints in compression (if compared with their shear stiffness) normal stresses on the base joint equilibrate the gravity forces. Maximum and minimum normal stresses on the base ($\sigma_{G_{z_1}}$ and $\sigma_{G_{z_2}}$) will be given by

$$\sigma_{G_{z_1}},\sigma_{G_{z_2}} = \gamma_r b + \frac{W_d}{el} \pm \frac{6W_d a}{l^2 e} \tag{14}$$

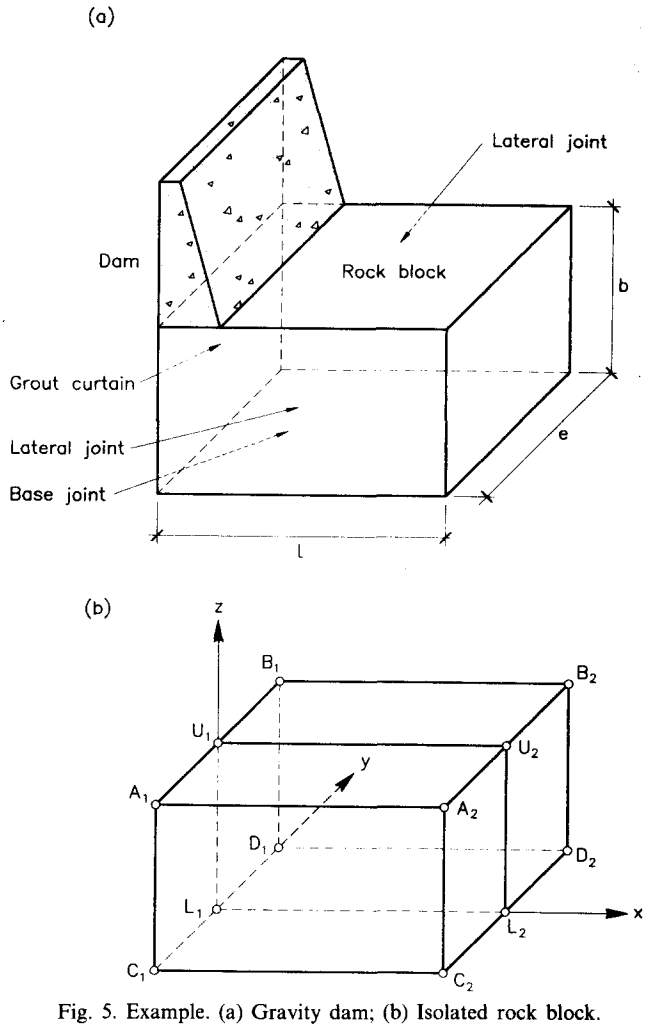

Fig. 5. Example. (a) Gravity dam; (b) Isolated rock block.

where W_d is the weight of the dam and a its arm with respect to the centre of the basal joint. According with the K_0 assumption the normal stresses on the lateral joint will be given by

$$\sigma_{G_y} = \left[\gamma_r(b - z) + \frac{W_d}{el}\right]K_0. \tag{15}$$

Hydrostatic "live" forces are separated in two parts: those acting on the dam vertical face [resultant, $\boldsymbol{E}_d = E_d\,(1, 0, 0)'$] and those acting on the upstream face of the rock block [resultant, $\boldsymbol{E}_r = E_r\,(1, 0, 0)'$] where

$$E_d = \tfrac{1}{2}\gamma_w h_w^2 e \tag{16}$$

$$E_r = \left(h_w + \frac{b}{2}\right)\gamma_w be \tag{17}$$

where γ_w is the unit weight of water.

These forces will induce a distribution of resisting shear forces (τ_E) on the surface S_1 (Fig. 6c). The determination of λ_E and λ_ϕ does not require the knowledge of τ_E. In fact their average value could be determined by imposing a condition of static equilibrium (along $\boldsymbol{d}$) but this is actually the condition leading to the determination of the safety factors. Once λ_ϕ is known, τ_E

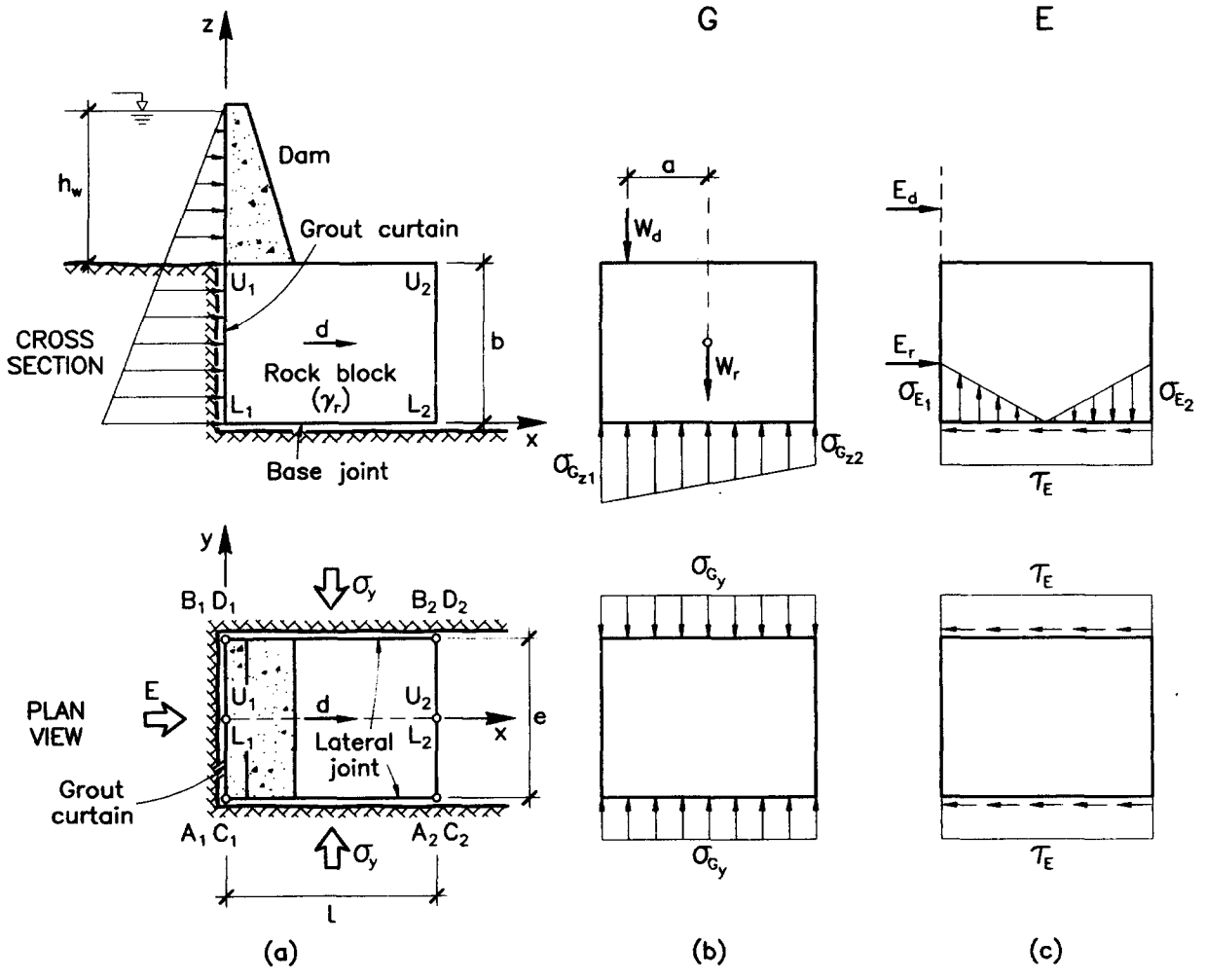

Fig. 6. Example. Gravity dam, vertical upstream face.

may be determined from equation (8) [$\tau^{mob} \equiv \tau_E$]. An antisymmetric distribution of normal stresses, with no component in the vertical direction is also induced by the forces $\boldsymbol{E}_d$ and $\boldsymbol{E}_r$.

The extreme values σ_{E_1} and σ_{E_2} are given by

$$\sigma_{E_2} = -\sigma_{E_1} = \frac{6M_E}{l^2 e} \tag{18}$$

where M_E is the moment of forces $\boldsymbol{E}_d$ and $\boldsymbol{E}_r$ with respect to the base. For simplicity reasons the assumption is here again that the moment of $\boldsymbol{E}$ forces is taken only by the base. When the analysis is performed numerically the stress–strain behaviour of joints and rock define the distribution of stresses.

Equation (5) will be used to find λ_E. Its different terms are given by

$$C = \int_{s_1} c \, ds = c(2bl + el) \tag{19}$$

$$N_E = \int_{s_1} \sigma_E \, ds = \int_{C_1 D_1 D_2 C_2} \sigma_E \, ds = 0 \tag{20}$$

$$N_G = \int_{s_1} \sigma_G \, ds = 2\int_{A_1 A_2 C_2 C_1} \sigma_{G_y} \, ds + \int_{C_1 C_2 D_2 D_1} \sigma_{G_z} \, ds$$

$$= (2K_0 \tfrac{b}{e} + 1)W_d + \gamma_r bl(e + K_0 b) \tag{21}$$

$$\boldsymbol{d}'\boldsymbol{G} = (1, 0, 0)\,(0, 0, -1)'(W_r + W_d) = 0 \tag{22}$$

$$\boldsymbol{d}'\boldsymbol{E} = (1, 0, 0)\,(1, 0, 0)'(E_r + E_d) = E_r + E_d. \tag{23}$$

Note that the distribution of σ_E on the base joint does not affect the results because it has a zero force resultant. However, if as a result of the moment M_E a part of the base joint tends to open, the surface S_1 will be modified. If equations (19)–(23), and (16) and (17) are introduced into equation (5) the following expression for λ_E is obtained after some simplification, assuming a cohesionless joint ($c = 0$):

$$\lambda_E = \frac{\gamma_r}{\gamma_w} \frac{\left[\dfrac{V_d}{ebl}\left(2K_0 \dfrac{b}{e} + 1\right) + \left(1 + K_0 \dfrac{b}{e}\right)\right] \tan \phi}{\dfrac{h_w}{l}\left(1 + \dfrac{h_w}{2b}\right) + \dfrac{b}{2l}} \tag{24}$$

where V_d is the volume of the dam and the same unit weight as for the rock is assumed for the dam material. In order to get some numerical values, consider the

following relative dimensions in this example: $V_d = 1/3$ ebl; $b/e = 2$; $h_w/b = 1$; $h_w/l = 1$. Then

$$\lambda_E = 3.22K_0 + 1.288. \tag{25}$$

Note that in this example

$$\lambda_E = \lambda_\phi = \frac{C + N_G \tan \phi}{\boldsymbol{d}' \boldsymbol{E}} \tag{26}$$

since $\boldsymbol{d}' \boldsymbol{G} = 0$ and $N_E = 0$.

Consider, however, the case in which the dam has an inclined upstream surface so that a nonzero average normal stress is induced by the hydrostatic load on the base joint. This case is illustrated in Fig. 7. If the dam has the same volume the "gravity terms" N_G and $\boldsymbol{d}' \boldsymbol{G}$ do not change. The hydrostatic load on the dam has now a horizontal component, E_{d_h}, given by equation (16) and a vertical one given by

$$E_{d_v} = \tfrac{1}{2}\gamma_w h_w^2 e \tan \alpha. \tag{27}$$

The distribution of normal stresses on the base joint changes and the extreme values σ_{E_1} and σ_{E_2} are given by

$$\sigma_{E_1}, \sigma_{E_2} = \frac{E_{d_v}}{el} \mp \frac{6M_E}{l^2 e} \tag{28}$$

where M_E is the moment of forces E_{d_v}, E_{d_h} and E_r with respect to the base. The term N_E now becomes

$$N_E = \int_{s_1} \sigma_E \, ds = \int_{C_1 D_1 D_2 C_2} \sigma_E \, ds = \tfrac{1}{2}\gamma_w h_w^2 e \tan \alpha. \tag{29}$$

The term $\boldsymbol{d}' \boldsymbol{E}$ has not changed because the inclination of the upstream face does not modify the horizontal hydrostatic force. The nonzero term N_E leads now to the following expressions for λ_E and λ_ϕ:

$$\lambda_E = \frac{\gamma_r}{\gamma_w} \tan \phi \, \frac{\dfrac{V_d}{ebl}\left(2K_0 \dfrac{b}{e} + 1\right) + \left(1 + K_0 \dfrac{b}{e}\right)}{\dfrac{h_w}{l}\left[1 + \dfrac{h_w}{2b}\left(1 - \tan \phi \tan \alpha\right)\right] + \dfrac{b}{2l}} \tag{30}$$

$$\lambda_\phi = \lambda_\phi^* + \tan \phi \tan \alpha \, \frac{\dfrac{h_w^2}{bl}}{2\dfrac{h_w}{l}\left(1 + \dfrac{h_w}{2b}\right) + \dfrac{b}{l}} \tag{31}$$

where λ_ϕ^* is the value given in equation (24) for a dam with vertical upstream face. For the example considered previously the following factors are now computed:

$$\lambda_E = 3.63K_0 + 1.46 \tag{32}$$

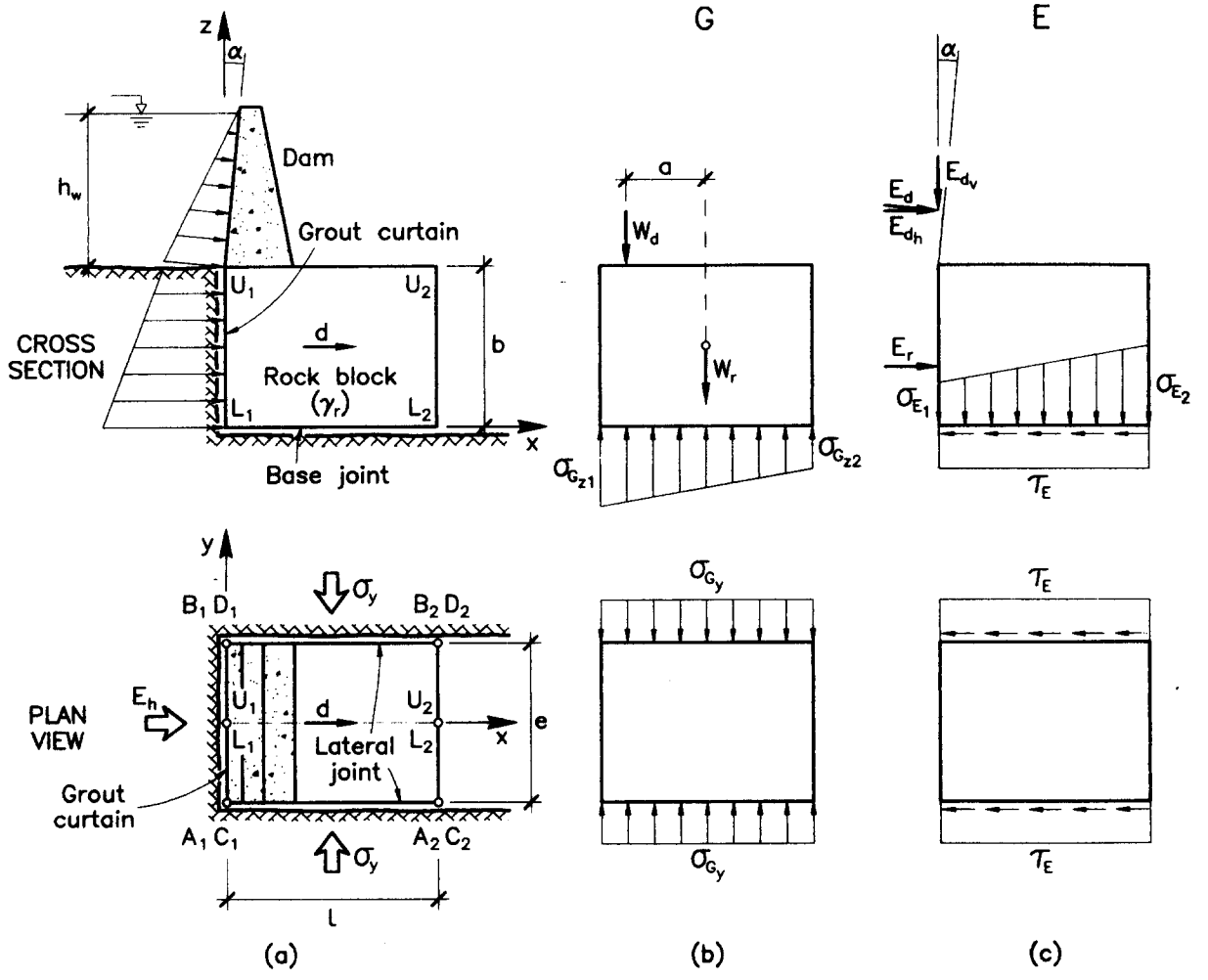

Fig. 7. Example. Gravity dam, inclined upstream face.

$$\lambda_\phi = 3.22K_0 + 1.405. \quad (33)$$

It can be seen now that $\lambda_E > \lambda_\phi$ and both are larger than the previously determined value. The reason is that the inclined upstream face of the dam introduces now a stabilizing force on the horizontal sliding joint.

MODELLING CANELLES DAM AND ITS FOUNDATION

Geometry

In view of previous experience and the needs of the safety analysis, a number of requirements for the 3D finite element mesh were put forward. It was decided to include:

(a) A sufficient portion of the rock mass surrounding the dam and a realistic representation of the abutments and the valley.
(b) a sufficient number of elements across the dam to capture bending.
(c) a sufficient number of joints of each family so that various failure mechanisms kinematically admissible could be considered and the most critical ones could be identified.
(d) joints in the concrete–rock interface.
(e) a continuous surface of element boundaries or joints representing the grout curtain.

In addition the size of the mesh (number of degrees of freedom) should not be too large in order to run the computations at a reasonable cost.

The discretized dam and its foundation in a view from downstream is shown in Fig. 8. Joints of the principal system (L1–L7 in the left margin and R1–R5 in the right margin) are shown in a vertical view in Fig. 9. The mesh has 1208 solid elements and 1505 joint elements. Due to the complexity of trying to approximate the real geometry, including a sufficient number of discontinuities, several types of solid elements have been required: hexahedron, prism (triangular base), pyramid (square base) and tetrahedron. Both quadrangular and triangular zero-thickness surface joint elements [7,8] were developed and used in the analysis. In total, 12 vertical joint planes belonging to the principal system of discontinuities and five bedding planes have been included in the discretization. Four additional horizontal planes have also been introduced to widen the range of possible failure mechanisms and to cover the event of nondetected discontinuities with unfavourable orientations.

To limit the number of degrees of freedom, linear elements have been used. However, this type of element prevents good reproduction of some parts of the geometry, especially that involving the arch dam itself. In order to discretize the dam, a superparametric element that allows a quadratic geometry definition and a linear displacement interpolation has been used (these elements were initially described by Zienkiewicz in 1971 [9]). In this way the total number of nodes of the mesh is 3586 (10,758 d.o.f.).

Joint model

A fairly comprehensive constitutive model for describing the 3D behaviour of rock joints was described by Carol *et al.* [6]. A hyperbolic failure criterion containing two parameters was adopted to define a family of yield surfaces. A general hardening/softening law and a flow rule that describes dilatancy as a function of stress and strain levels was defined. Locking behaviour in compression and load/unloading cycles could be modelled as well as anisotropic characteristics of the joint. This model is able to reproduce experimental results [6,7] with high accuracy (Fig. 10). The numerical implementation of the model requires, however, a relatively complex integration procedure in order to take into account different modes of joint behaviour. An isoparametric joint model was also developed in connection with this constitutive law and its performance as an interface element was examined in some detail in Gens *et al.* [8].

When the number of degrees of freedom is large, it is convenient to reduce the computational effort. One of the advantages of the constitutive joint model described in ref. [6] is that an explicit version can be derived if some simplifying assumptions are introduced. These are: (a) perfect elasto-plastic behaviour; (b) linear relationship between normal stress and normal displacement and (c) no dilatancy. A hyperbolic yield surface is maintained. With these assumptions the stress–strain law can be integrated analytically, allowing a significant reduction of computer cost when compared to the full constitutive law, which requires numerical integration.

This is a distinctive advantage when a detailed geometry of the rock mass is required in order to reproduce unstable mechanisms. The simplified joint constitutive model is described in the Appendix.

Stages of the analysis

A computer code called Code DRAC, described in Prat *et al.* [10] was used to perform the 3D finite element analysis. Four construction stages were defined: the first stage simulates the initial state of the rock, before building the dam. In this stage the weight of the rock was applied in increments. Two values of the "at rest pressure coefficient", K_0, were considered: a relatively low value ($K_0 = 0.43$) which is perhaps conservative from the point of view of the stability of the jointed rock and a higher value, $K_0 = 0.9$. The influence of K_0 on the dam safety could then be analyzed for this range of values. Selfweight was applied in 10 increments in the first case and 12 in the second one.

The dam and counterfort on the right abutment were built in three additional stages which roughly correspond to 1/3, 2/3 and 3/3 of the height of the structures put in place (Fig. 11).

At each stage all the elements of the new layer are added and their corresponding weight applied. Each of the three construction stages involved the application of the load in 10 increments (10% of the total weight in each case). This construction sequence which is convenient for the numerical analysis does not reproduce in

8

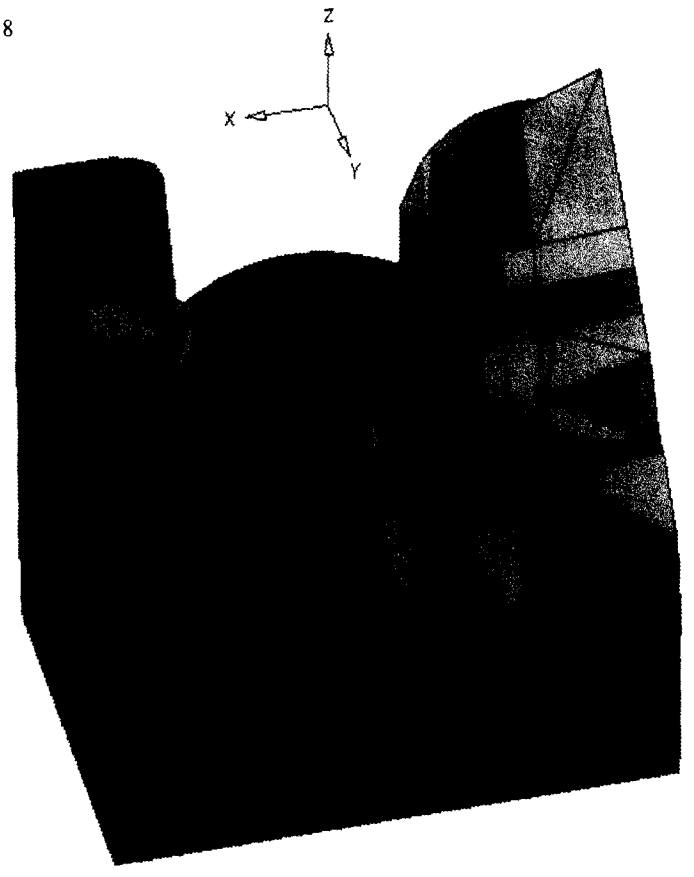
Z
X
Y

Fig. 8.

9

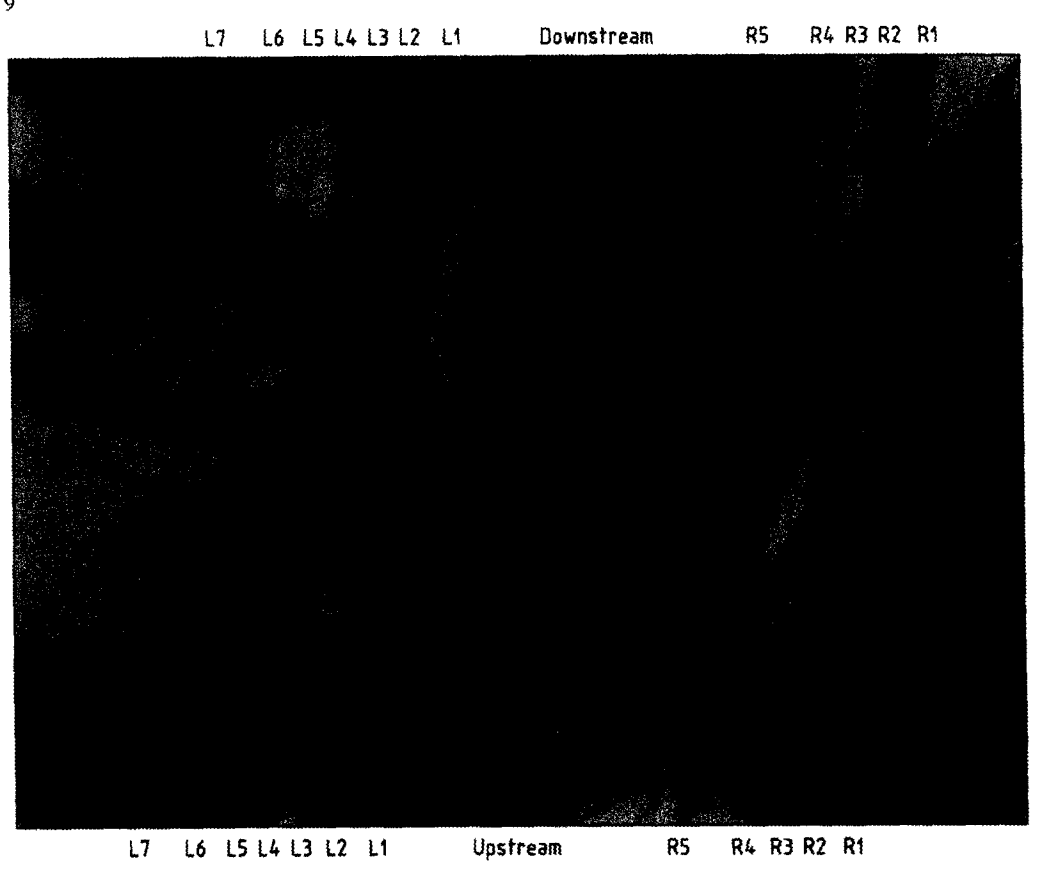
Y
X
Z
L7 L6 L5 L4 L3 L2 L1 Downstream R5 R4 R3 R2 R1
L7 L6 L5 L4 L3 L2 L1 Upstream R5 R4 R3 R2 R1

Fig. 9.

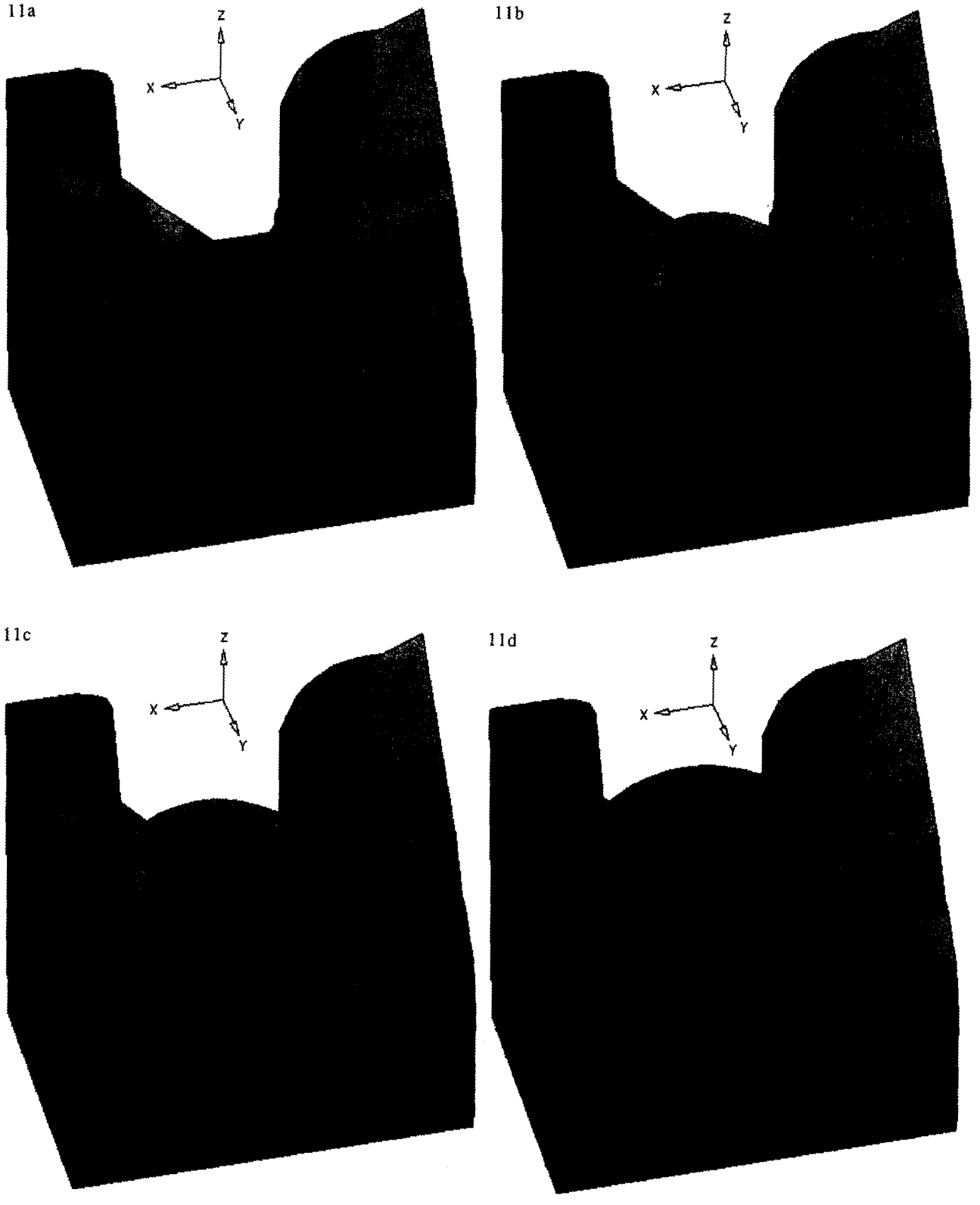

Fig. 11.

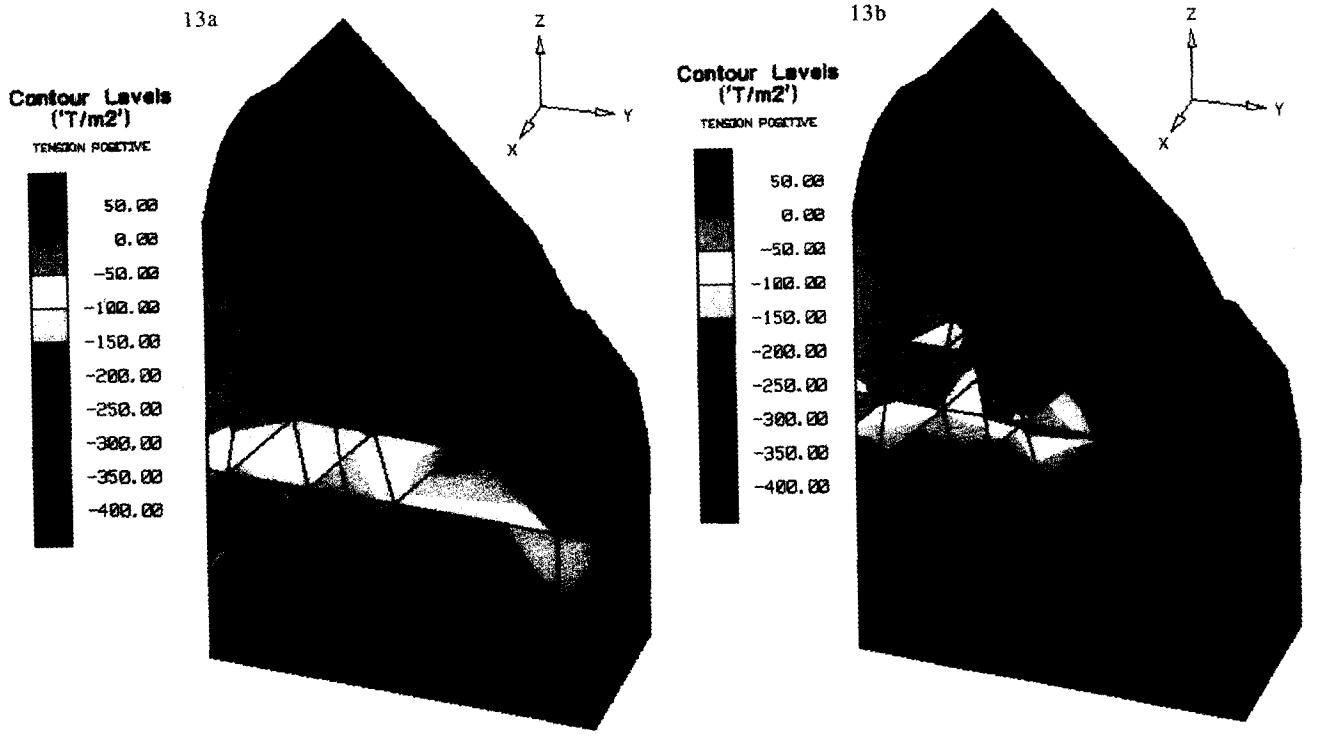
13a
Contour Levels
('T/m2')
TENSION POSITIVE
50.00
0.00
-50.00
-100.00
-150.00
-200.00
-250.00
-300.00
-350.00
-400.00
Z
Y
X
13b
Contour Levels
('T/m2')
TENSION POSITIVE
50.00
0.00
-50.00
-100.00
-150.00
-200.00
-250.00
-300.00
-350.00
-400.00
Z
Y
X

Fig. 13.

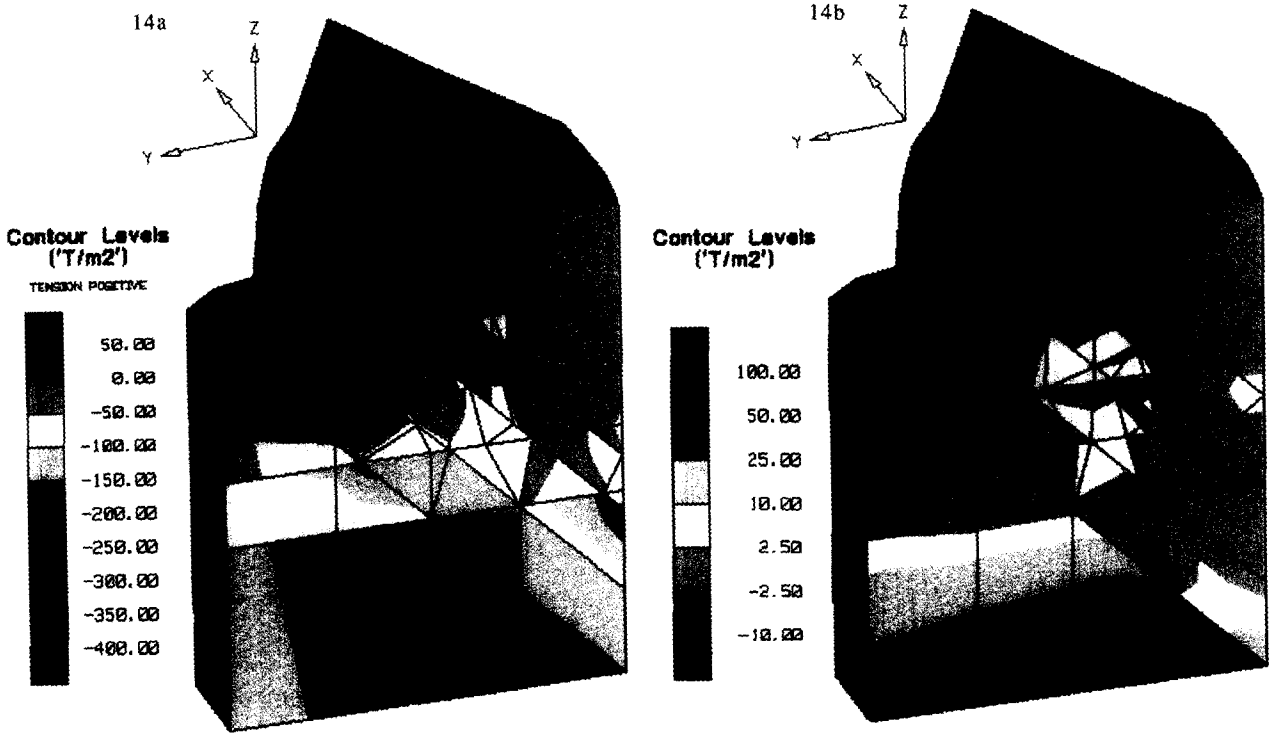
14a
Contour Levels
('T/m2')
TENSION POSITIVE
50.00
0.00
-50.00
-100.00
-150.00
-200.00
-250.00
-300.00
-350.00
-400.00
Z
X
Y
14b
Contour Levels
('T/m2')
100.00
50.00
25.00
10.00
2.50
-2.50
-10.00
Z
X
Y

Fig. 14.

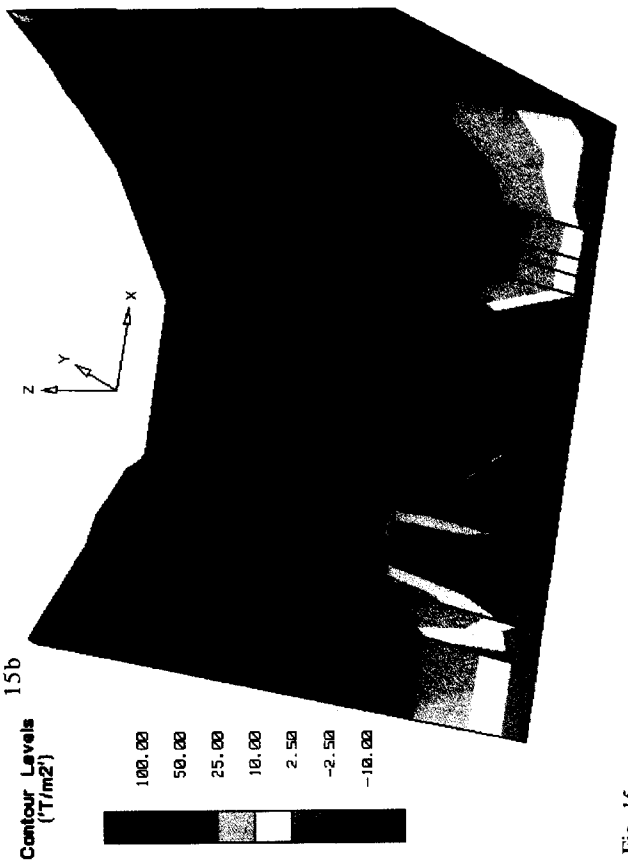
15b
Contour Levels
('T/m2')
100.00
50.00
25.00
10.00
2.50
-2.50
-10.00
Z
Y
X

Fig. 15.

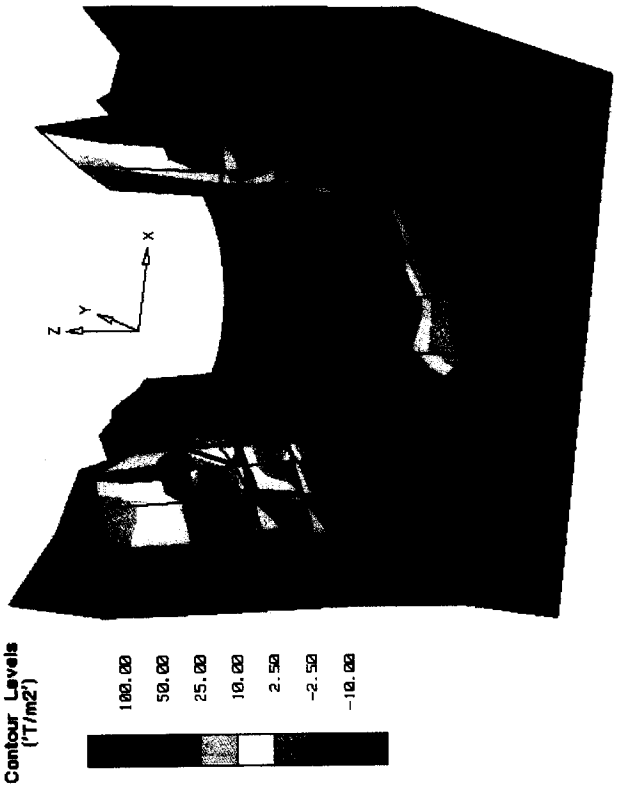
16b
Contour Levels
('T/m2')
100.00
50.00
25.00
10.00
2.50
-2.50
-10.00
Z
Y
X

Fig. 16.

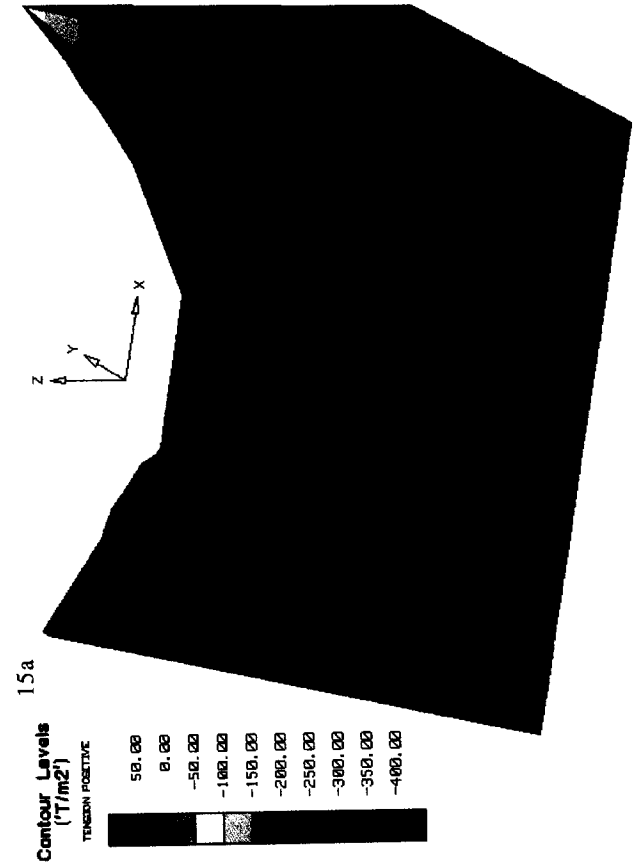
15a
Contour Levels
('T/m2')
TENSION POSITIVE
50.00
0.00
-50.00
-100.00
-150.00
-200.00
-250.00
-300.00
-350.00
-400.00
Z
Y
X

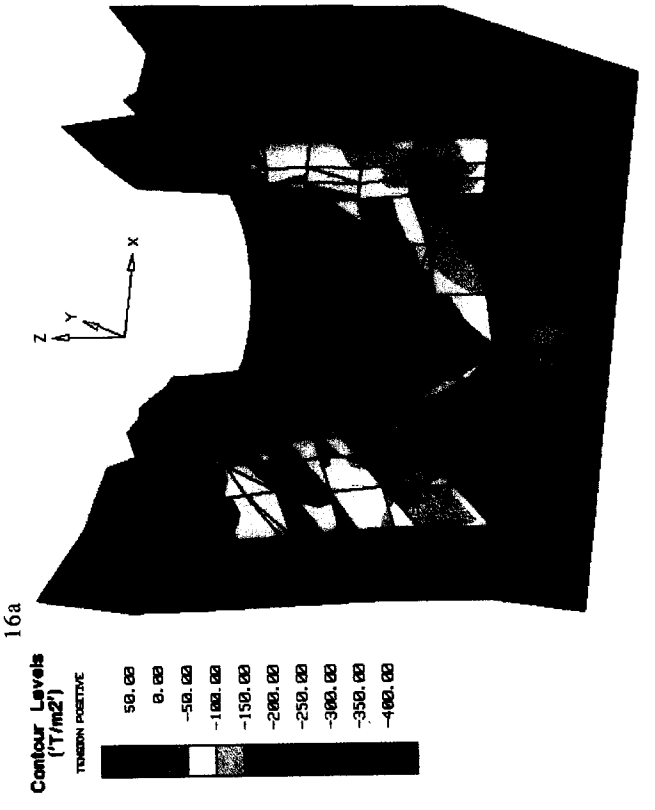
16a
Contour Levels
('T/m2')
TENSION POSITIVE
50.00
0.00
-50.00
-100.00
-150.00
-200.00
-250.00
-300.00
-350.00
-400.00
Z
Y
X

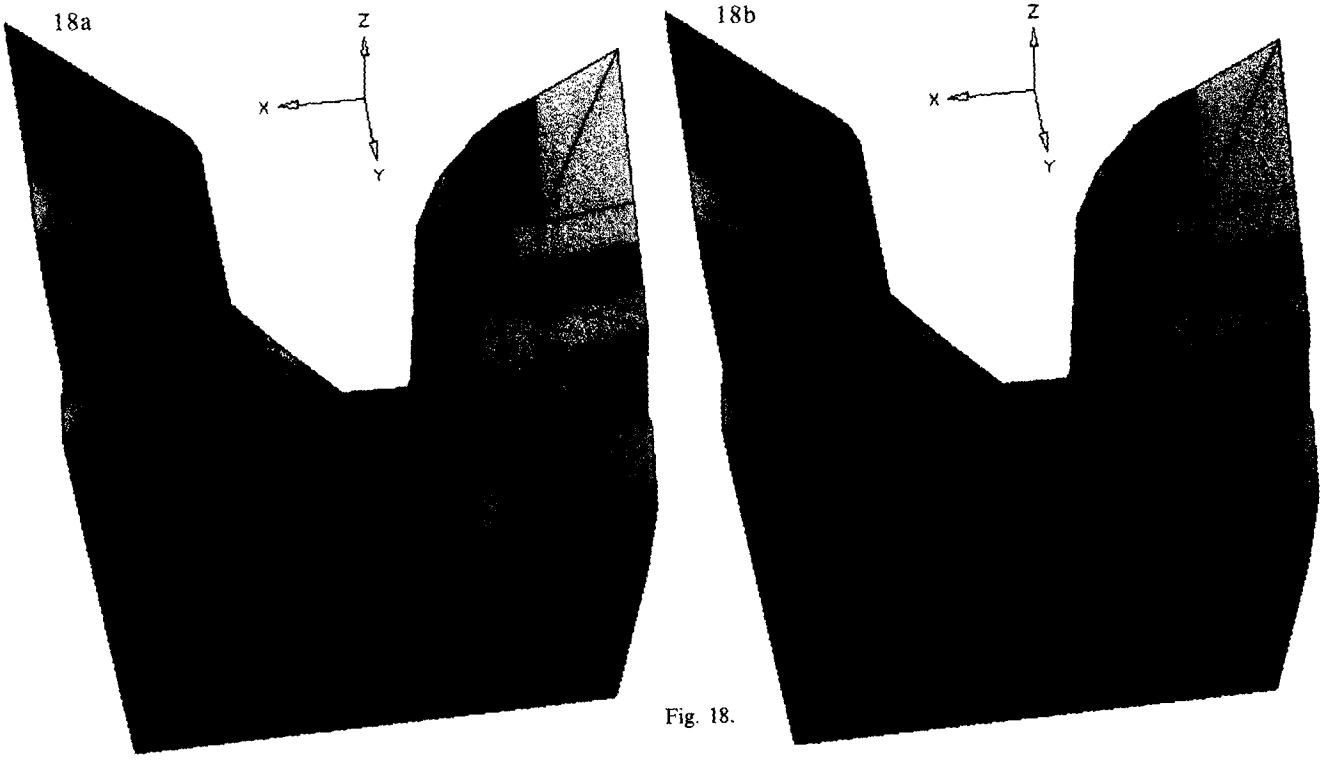

Fig. 18.

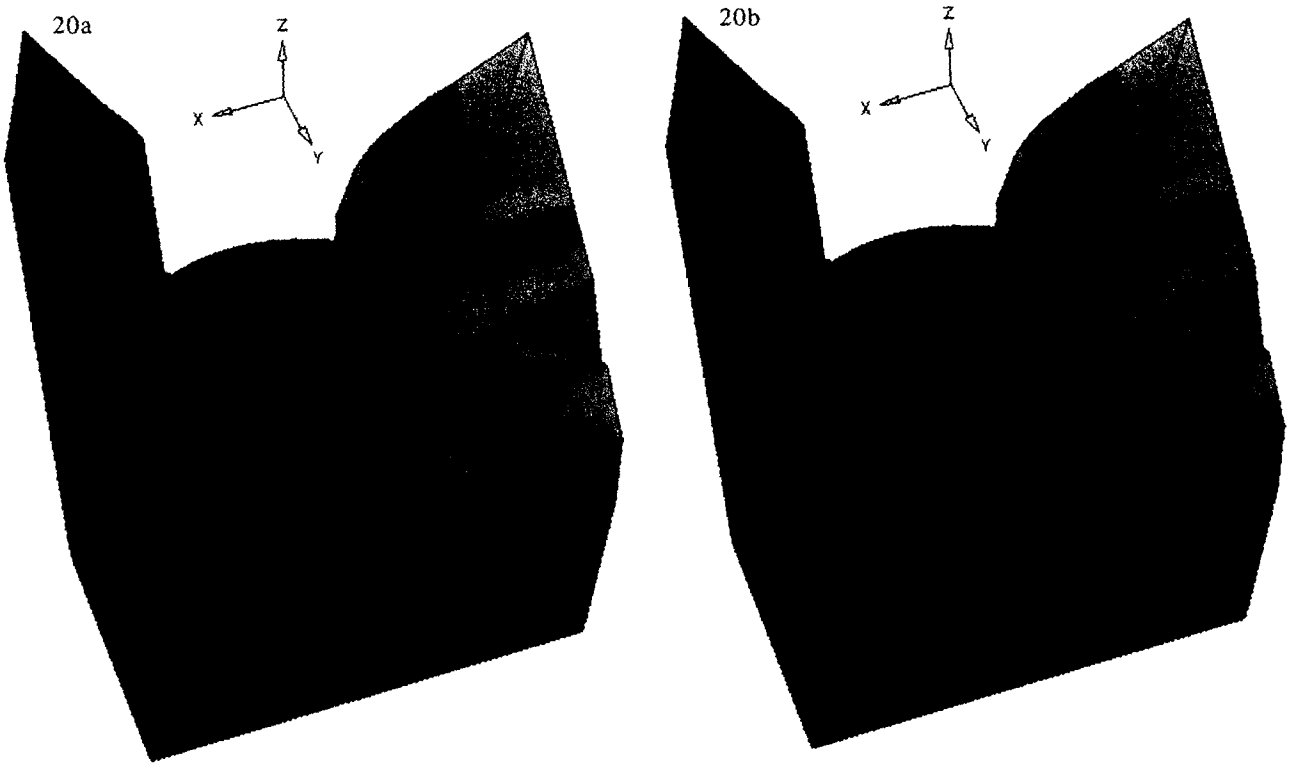

Fig. 20.

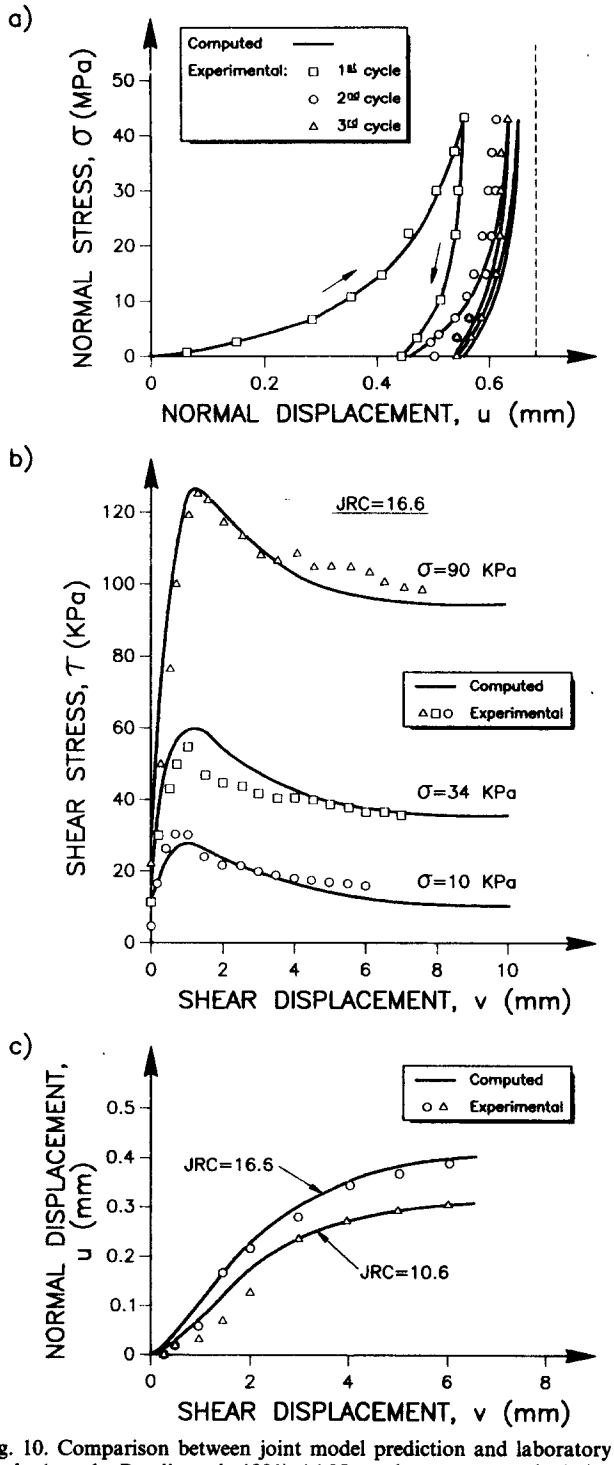

Fig. 10. Comparison between joint model prediction and laboratory results (tests by Bandis et al., 1981). (a) Normal stress—normal relative displacement curves. (b) Tangential stress—tangential relative displacement curves. (c) Dilatancy curves.

detail the actual construction history of the dam and counterfort (the counterfort was built after the dam was erected and not simultaneously). It is believed, however, that the errors introduced in the actual stress distribution by the construction sequence adopted in the model should be small.

The hydrostatic load against the dam and the upstream grout curtain was applied as a loading step of the final construction stage in 20 increments of 5% of the total pressure. Water pressure was assumed to remain constant below the deepest foundation level because of the presence of a stable water level downstream of the dam.

Given the nonlinearity of the problem, all the loads (self-weight and hydrostatic load) were applied in small increments. This is specially relevant in problems with a complicated geometry such as steep wall canyons where large stress gradients are to be found across small distances.

The Young's moduli of the rock used in the analysis were derived from back calculations of the dam performance for two water levels in the reservoir for which deformations of the abutments were measured. It was found that the rock moduli varied from 6.3 GPa at higher elevations to 19 GPa for the deeper rock mass.

Large scale *in situ* shear tests on joints of the principal system and bedding planes provided the data to select the parameters of the hyperbolic strength envelope of the joints constitutive model. Residual strength values differ by a small amount from the peak values and the latter were selected to avoid an over pessimistic attitude, since rock bridges, present in many joints have been disregarded in the analysis. The following strength parameters were derived from the tests $c = 0.124$ MPa; $\phi = 18.7°$ for joints of the principal system and $c = 0.135$ MPa; $\phi = 35.2°$ for the bedding planes ($c = a \tan \phi$) [See Fig. A2 of the Appendix for the definition of c]. The corresponding hyperbolic strength envelopes are shown in Fig. 12.

For the remaining joints and interfaces of the model (horizontal planes, grout curtain and rock–concrete interfaces) the values corresponding to bedding planes were adopted. This decision was taken in view of the roughness and soundness of these planes, which are presumably more akin to the clean bedding planes than to the clay-filled joints of the principal system.

Normal and shear stiffness moduli of all the joints (K_n and K_t) have deliberately been taken high ($K_n = K_t = 10^5$ MPa) in order to ensure the continuity of both sides of the joint if the shear stress does not reach the shear strength values.

At each iteration of the computations the presence of residual stresses implies the existence of incompatible stress states. The iteration process reduces the amount of residual stresses to a level that was controlled by means of a convergence index. A convenient choice is to relate the Euclidean norm of the vector of residual forces of the last iteration of a given loading increment (N) with the norm of the vector of external forces and nodal reactions applied at the same increment N. This convergence index is given in Table 1 for the final loading step of the construction stages defined previously.

Table 1. Convergence index (%)

Stage	Description	N	Convergence index (%) $K_0 = 0.43$	$K_0 = 0.9$
1	Self weight	10/12	0.69	0.43
2	1/3 dam	10	1.61	2.3
3	2/3 dam	10	3.6	4.3
4	3/3 dam	10	6.7	5.1
4.1	Hydrostatic load	20	5.1	2.3

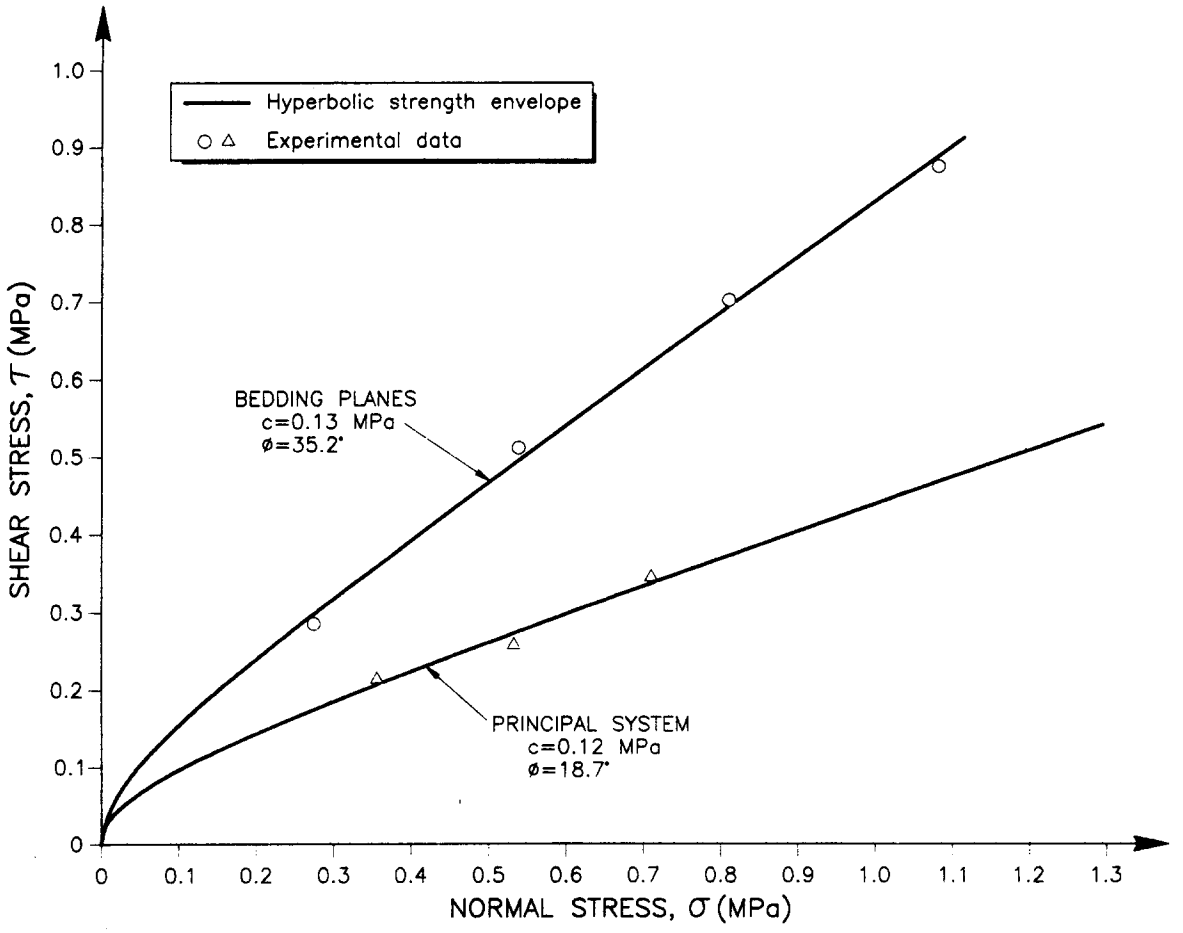

Fig. 12. Hyperbolic strength envelopes for joints of the principal system and bedding planes.

Convergence conditions seem to improve for higher values of K_0. In any case, the values given in Table 1 show that the amount of unbalanced loads with respect to the external loads and nodal reactions is sufficiently small for practical purposes.

Illustrative results

Three-dimensional analyses require powerful post processors to handle the massive information provided by the FE computations. The code DRAC is linked to a postprocessor program, DRACVIU, which provides a wide range of plotting capabilities for examining the results at each stage of the analysis. The most relevant information to be obtained concerns the stress distributions on all the discontinuities since they are directly related to the sliding mechanisms. A detailed examination of the stresses on the discontinuities has led to a better understanding of the resistance mechanisms of the dam foundations and to a rational identification of failure mechanisms. These mechanisms will be discussed in the next section.

The initial state of stress due to selfweight (state 1 of the computation) showed a consistent pattern. Normal stresses on vertical joints such as I3 on the left abutment for $K_0 = 0.43$ and $K_0 = 0.9$ (Fig. 13a,b) increased with depth, reflecting the topography. Some (small) tension stress states remained in shallow rock blocks, adjacent to the vertical canyon walls. The value of K_0 affects the results (compare Fig. 13a and b), especially at depth. At higher elevations close to the canyon walls boundary conditions tend to control the results and the distribution of initial stresses is not particularly affected by K_0.

Construction of the dam increases normal stresses in the abutments. A typical upstream displacement of the structure was computed. Application of the full hydrostatic pressure leads to a profound modification of the state of stress in the structure, and in some joints and interfaces.

It is interesting to examine the stress conditions of some joint planes in the rock mass when the full hydrostatic load is applied. Figure 14a,b shows the distribution of normal stress and available shear strength or local safety margin (the difference between the shear strength and the computed shear stress) for vertical joint D3 in the right abutment ($K_0 = 0.43$). At high levels of local safety margin is small but it increases at depth. A similar plot for one of the sedimentary planes (which dip 45° upstream) is shown in Fig. 15a,b ($K_0 = 0.43$). It can be seen in Fig. 15b that upstream of the grout curtain negative local safety margins are computed. However, most of the surface of these bedding planes, downstream of the front curtain, exhibits a significant strength reserve.

It is also interesting to examine the situation of the grout curtain, which directly receives the hydrostatic load (the load was applied to the solid elements downstream of the curtain, represented by joint elements).

Table 2. Safety factors from nonlinear stress–strain analysis

Family of mechanism	Type of safety factor	Initial stresses $K_0 = 0.43$	Initial stresses $K_0 = 0.9$
(a) Global	λ_E	4.35–4.96	5.17–6.02
both abutments	λ_ϕ	3.02–3.64	4.11–4.57
(b) Local	λ_E	3.13–6.52	3.14–11.05
left abutment	λ_ϕ	2.47–3.67	2.17–5.24
(c) Local	λ_E	6.31–7.72	6.60–8.16
right abutment	λ_ϕ	3.85–4.21	4.88–5.28
(d) Along	λ_E	6.15–7.90	5.50–6.40
bedding planes	λ_ϕ	−1.44; −5.10	−1.80; −10.16

Figure 16a represents the distribution of normal stresses for $K_0 = 0.9$. Some tension zones are computed. A parallel plot of available shear strength is shown in Fig. 16b. These plots are useful to identify failure mechanisms and to understand the behaviour of dam foundations.

SAFETY ANALYSIS

Safety factors from nonlinear analysis

The determination of factors of safety is a capability of the postprocessing module DRACVIU. It is possible to perform interactively the selection of failure mechanisms and sliding directions as well as the computation of the corresponding factors of safety according to expressions given before. The same routines used in the definition of parts of the mesh required for plotting are in fact employed to select the desired failure mechanisms. In DRACVIU the user may select part of the mesh as a potential failure mechanism. To assist in a proper selection, the program plots the remaining geometry. The potential failure surface is then easily identified. Two examples of analyzed mechanisms are given in Figs 18 and 20.

Many different potentially unstable mechanisms were considered and they may be grouped into four categories:

(a) Global mechanisms affecting the two abutments. They are bounded by two or more vertical joints (principal system) and one or more horizontal discontinuities. They affect the dam as a whole. The sliding direction is determined by the orientation of the vertical discontinuities.

(b) Left abutment mechanisms. Bounded by vertical and horizontal planes. Sliding direction $\boldsymbol{d}$ is given by the strike of the principal system.

(c) Right abutment mechanisms. Bounded by vertical and horizontal planes. Sliding direction $\boldsymbol{d}$ is given by the strike of the principal system.

(d) Local or global mechanisms involving bedding planes.

Figure 17 provides a simplified geometrical representation of 16 global mechanisms and the associated safety factors λ_E and λ_ϕ computed through equations (7) and (13) for $K_0 = 0.43$. Thirty-two global mechanisms were examined and the minimum computed values for the safety factors are:

$$\lambda_E = 4.35 \text{ (mechanism 23; } K_0 = 0.43)$$

$$\lambda_\phi = 3.02 \text{ (mechanism 28; } K_0 = 0.43).$$

Mechanism 28 is illustrated in more detail in Fig. 18.

Thirty-two local failure mechanisms in left abutment were also examined. The simplified shape and associated safety factors for the first 16 mechanisms and $K_0 = 0.9$ are shown in Fig. 19. The minimum computed values are:

$$\lambda_E = 3.13 \text{ (mechanism 22; } K_0 = 0.43)$$

$$\lambda_\phi = 2.17 \text{ (mechanism 7; } K_0 = 0.9).$$

Mechanism 7 is illustrated in Fig. 20.

The analysis was completed by a limited number of (5) failure mechanisms in the right abutment (it was found significantly safer than the left one) and three additional mechanisms involving bedding planes which exhibited very high safety factors.

It was consistently found that some mechanisms involving wedges in the left abutment led to the lowest safety factors.

A summary of the range of values computed for all the sliding mechanisms analyzed as a function of the K_0 value is given in Table 2.

Table 3. Computed safety factors for an external load equal to three times the hydrostatic pressure

Family of mechanism	Type of safety factor	Initial stresses $K_0 = 0.43$	Initial stresses $K_0 = 0.9$
(a) Global	λ_E	2.82–3.99	2.71–3.81
both abutments	λ_ϕ	1.90–2.10	2.14–2.41
(b) Local	λ_E	1.51–4.74	1.60–4.30
left abutment	λ_ϕ	1.30–2.48	1.35–2.98
(c) Local	λ_E	4.65–7.72	3.53–5.08
right abutment	λ_ϕ	2.31–2.48	2.50–2.79
(d) Along	λ_E	11.9–100	4.28–13.3
bedding planes	λ_ϕ	−17.3; −4.07	7.06; −4.62

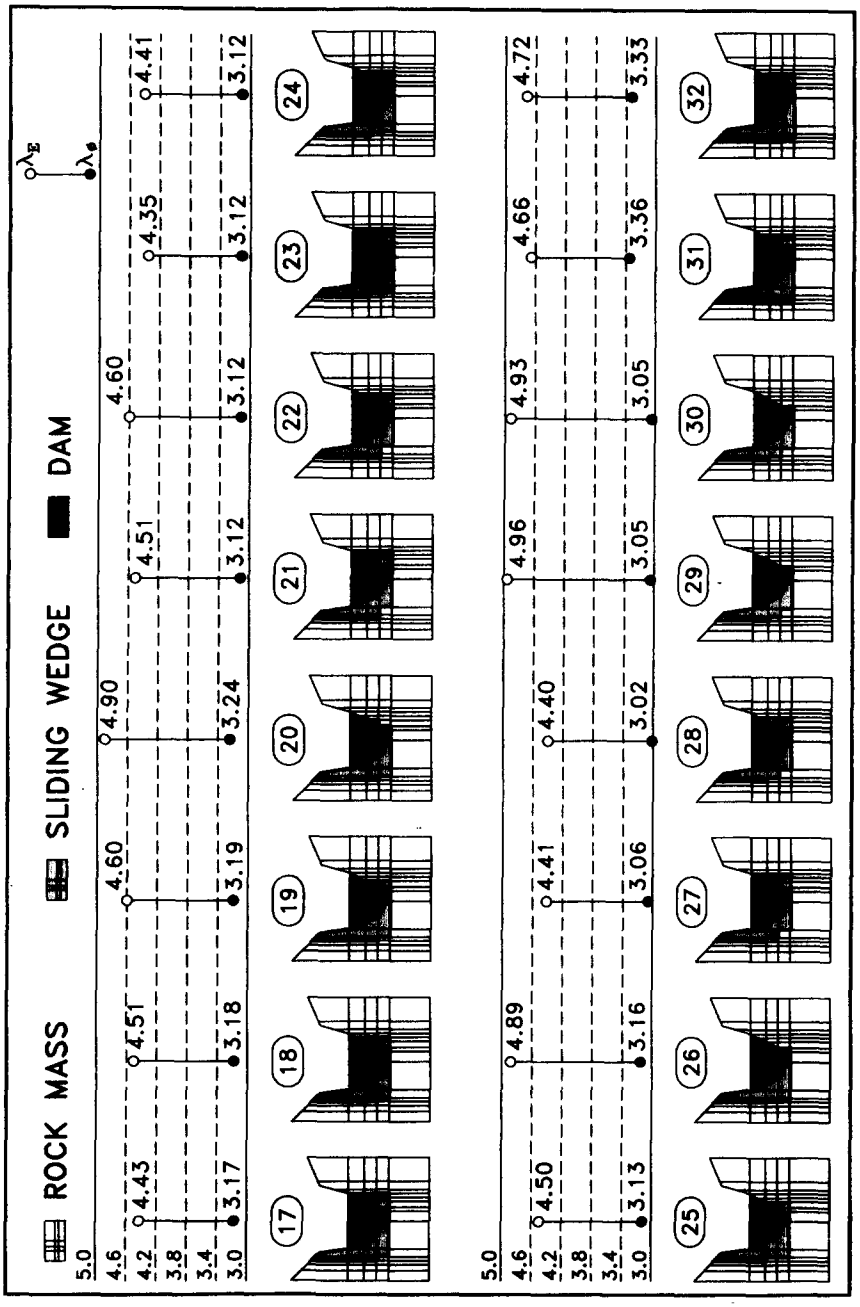

Fig. 17. Global failure mechanisms and associated safety factors (nonlinear analysis, $K_0 = 0.43$; failure mechanisms 17 to 32).

Negative values have been computed for λ_ϕ when analyzing failure mechanisms along bedding planes (which dip upstream). This is an indication of an impossible mechanism (wedges are stable against sliding on bedding planes under hydrostatic load, independent of the value of strength parameters).

Based on Table 2 the influence of initial stresses cannot be established with certainty. Most of the time, however, minimum values of safety factors are found for the lower value of K_0. Exceptions to this general trend have been found in some local failure mechanisms of the left abutment.

Failure load

In order to evaluate the ultimate failure load the nonlinear analysis has been continued after the final stage (self-weight plus hydrostatic load) adding load increments of 5% of the hydrostatic pressure until the total applied load reached a value of three times the nominal maximum hydrostatic pressure, P_h. The convergence index defined before exhibited acceptable values during this loading process (Fig. 21) for $K_0 = 0.43$. In fact, failure conditions, which could be identified by poor convergence, were not reached during this loading process. An examination of the stresses and deformations with increasing water pressure showed clearly how the dam and its foundation behaved. Increasing compression on the vertical joints close to the abutments led to its progressive closing.

The rate of increase of horizontal deformations with external load was greatest in the dam itself and decreased rapidly inside the rock abutment.

At each stage of the applied load, safety factors λ_E and λ_ϕ were also computed. Their evolution gives an interesting indication of the overall strength reserve offered by the rock foundation. As an illustration, Figs 22 and 23 show the change in λ_E and λ_ϕ with applied load for two of the most critical mechanisms in terms of λ_E identified in the previous analysis (mechanism 23 for the global family in Fig. 22 and mechanism 7 for the left abutment in Fig. 23).

Some conclusions may be derived from these plots. It is clear that the application of an externally increasing load results in a redistribution of internal stresses in the fractured rock which is insufficiently accounted for by the hypothesis leading to the definition of safety factor λ_E. In fact, according to Table 2, a load increment factor of $\lambda_E = 3.13$ should take the most critical wedge of the left abutment very close to failure conditions. For a load factor of 3, however, the range of computed values for λ_E is 1.51–4.74 if $K_0 = 0.43$, and 1.60–4.30 if $K_0 = 0.9$ (see also Table 3).

Figures 22 and 23 also indicate that the influence of initial stress, as given by K_0, is progressively lost as the water pressure increases. This is an indication of the smaller importance of initial normal stresses on relatively shallow joints when compared with the load-induced values.

Minimum and maximum values of computed safety factors for a load equivalent to three times the hydrostatic pressure are given in Table 3. The reduction observed in λ_E and λ_ϕ when the load increases, if compared with equivalent values in Table 2, is not explained by a "proportional" change in internal stresses.

This means that normal stresses on critical joints increase at a faster rate than the proportional increase in applied hydrostatic load. This mechanism results in a larger available strength than the strength implied by the hypothesis introduced in equation (3) and therefore in an improvement of the safety of the dam over the safety implied by the safety factor λ_E.

In terms of λ_ϕ (a safety measure which is probably to be preferred since it reflects the uncertainties in strength parameters and not a physically impossible event as embodied in λ_E), Table 3 indicates that the minimum safety factors are computed for $K_0 = 0.43$.

It is quite unlikely that K_0 in a cretaceous limestone outcrop reaches smaller values. Therefore, it can be concluded that the foundation of Canelles dam has a satisfactory level of safety.

CONCLUSIONS

Appropriate safety margins are an important design requirement for the foundation of structures in fractured rock. However, it is not a straightforward procedure to interpret the results of finite element analysis in terms of safety factors. This topic has been discussed in this paper in connection with the analysis of a large arch dam and its foundation on fractured limestone. The procedure developed has benefited from a long term research effort which has involved simplified 2D analysis, a detailed geometrical representation of the fractured rock, its main discontinuities and the relevant interfaces (rock–structure contacts; grouting curtains), linear and nonlinear analysis of the initial state of stress, construction sequence and application of the hydrostatic load and, finally, the definition and computation of safety factors. Some conclusions reached during this study are:

—Two alternative definitions of safety can be defined. The first measure (λ_E) is a multiplicative factor of the imposed external loads, whereas the second (λ_ϕ) is a reduction coefficient of the available strength on joints and interfaces. In both cases the factor is computed by establishing limiting equilibrium conditions of some selected failure mechanism. The second factor, λ_ϕ, is directly related to our uncertainty in strength parameters and has a more reasonable conceptual basis than λ_E. Consistently, the computed values of λ_E are larger than the values of λ_ϕ for all of the different mechanisms and states of initial stress analyzed.

—The defined safety factors may be computed for linear as well as nonlinear stress–strain analysis. In fact, a relatively cheap elastic finite element analysis of the dam construction and hydrostatic loading provides sufficient data to estimate the safety factors as a first approximation. An important requirement for this safety analysis, however, is the necessity to identify

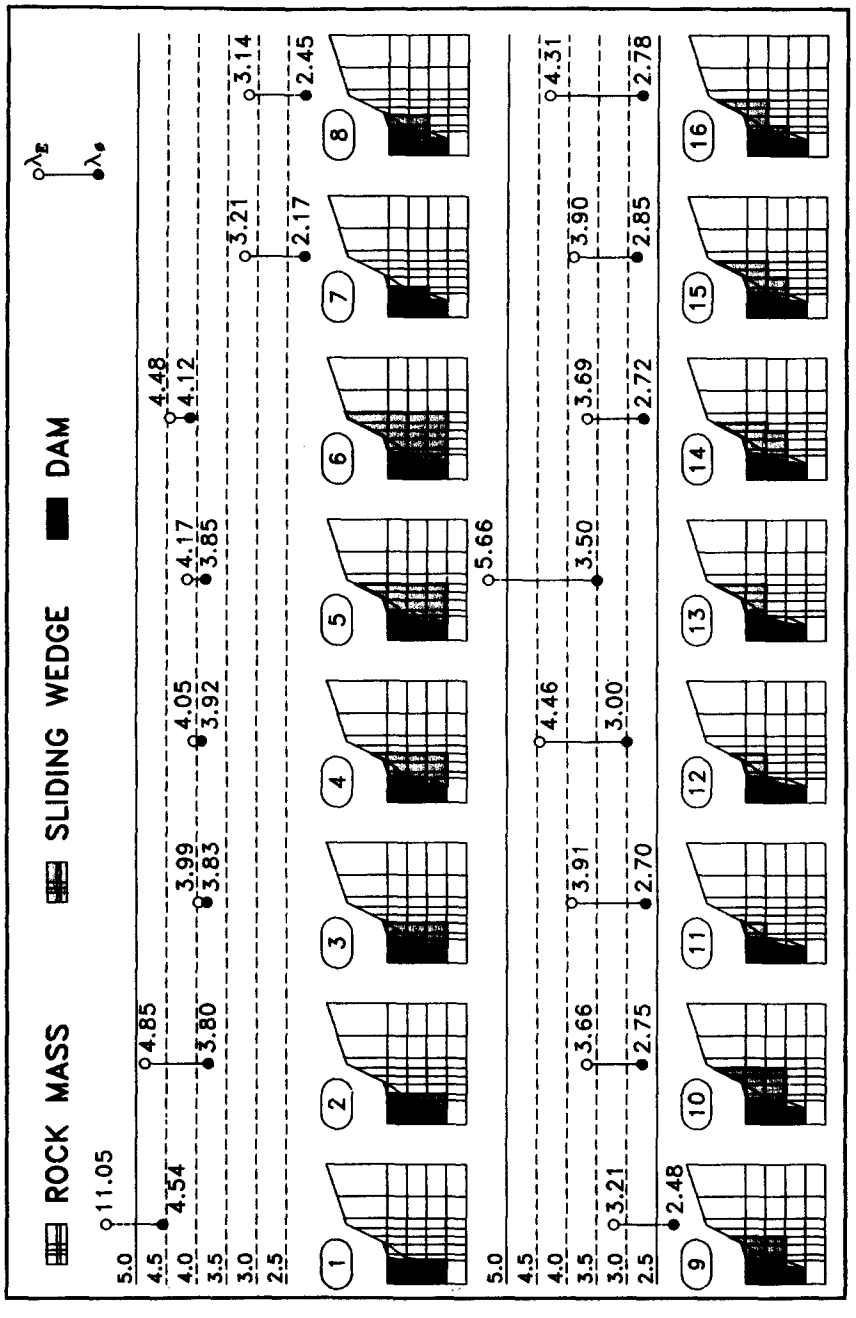

Fig. 19. Local failure mechanisms of left abutment and associated safety factors (nonlinear analysis, $K_0 = 0.90$; failure mechanisms 1 to 16).

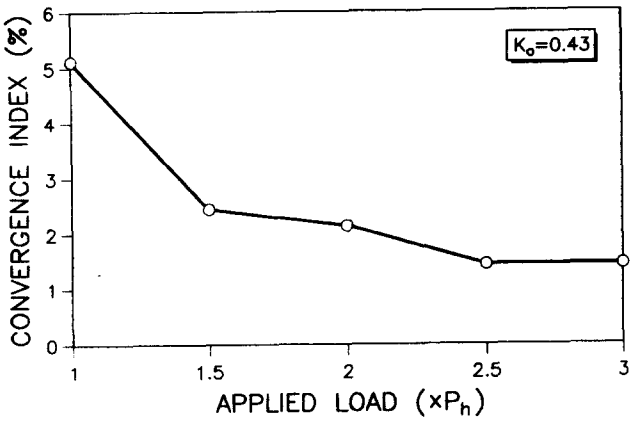

Fig. 21. Evolution of convergence index with applied load ($K_0 = 0.43$).

failure mechanisms. This may be achieved for instance, by examining the available shear strength along joints and interfaces. In practice it is more convenient to select by inspection blocks of the rock mass (and structure) bounded by the built in joints and interfaces. An appropriate postprocessing software such as DRACVIU in the case discussed in the paper is an invaluable aid in this regard.

—An examination of the evolution of safety factors as the external load increases (nonlinear analysis) has revealed that the initial estimation of safety factors for the nominal hydrostatic load provides a conservative set of values, in the sense that the redistribution of stresses associated with the increasing load provides additional strength reserves to sliding.

—The initial state of stress affects the safety factor of unstable mechanisms. It is, however, difficult to predict since the value and distribution of K_0 remains uncertain unless precise and comprehensive *in situ* measurements are available. It has been shown that lower values of K_0 imply lower safety factors

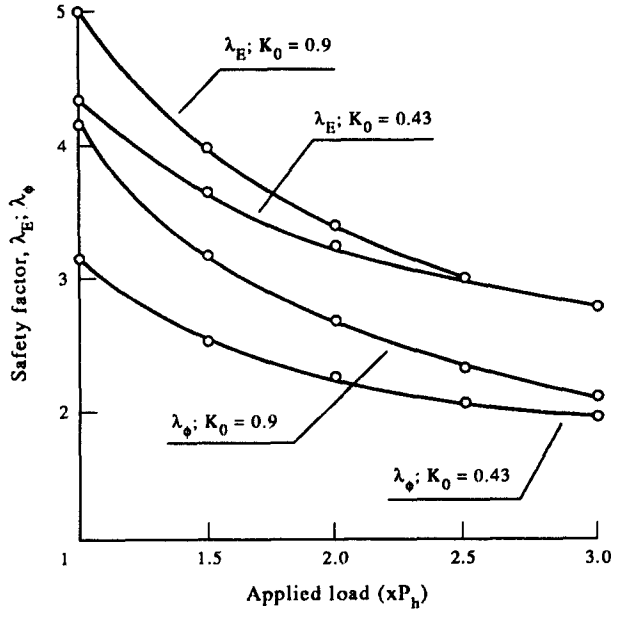

Fig. 22.

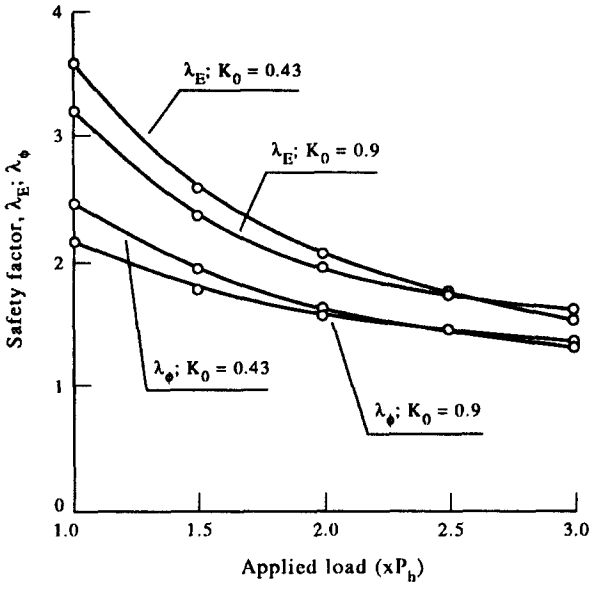

Fig. 23.

although the reverse is true for some isolated failure mechanisms. In the case analyzed, and due probably to the strong effect of canyon geometry in controlling the stresses in both abutments, the difference in safety for the two extreme values considered ($K_0 = 0.43$ and $K_0 = 0.9$) is not very significant. When the external load on the dam increases over the hydrostatic pressure, approaching ultimate states, the memory of the initial stress state is lost and the difference in safety factors for different initial K_0 values reduces. For a load equal to three times the hydrostatic pressure, the difference in computed safety factors has been very much reduced.

A few final comments may be made regarding the demands, in terms of reconnaissance effort and computer work required in practice, to apply the method described. A reliable determination of joint strength parameters is an obvious requirement of the analysis but this is always the case in rock mechanics when limiting conditions are examined. Computed safety factors also depend on the specific geometric representation of the rock mass and, in particular, on the position of the joint surfaces. Possible failure mechanisms depend on this basic representation. Missing a significant feature may also imply missing a critical failure mechanism and therefore overestimating the actual reliability of the structure. Regarding computer analysis it is felt that complicated geometries are not easily handled by mesh generation routines. In the case described a full manual discretization of the dam and its foundation was carried out. No less than four man-months of a highly skilled analyst were required. The application of the method requires also a postprocessing software which allows the selection of failure mechanisms. Experience has shown that the search for minimum safety factors is not the most difficult part of the procedure. After some trials the

location and type of critical wedges may be readily identified. In the case of Canelles dam they were located on the left abutment and corresponded to relatively small rock wedges acted by the thrust of the concrete dam.

An additional significant factor controlling the computed safety factors is the *in situ* state of stress. This was clearly shown in a previous paper [5]. *In situ* stress conditions are not established by the analysis even if a full 3D modelling is carried out. Field determination and/or sensitivity analysis (as presented in this paper) are ways to increase the reliability of the analysis.

Acknowledgements—The financial support provided by the Empresa Nacional Hidroeléctrica del Ribagorzana and the Spanish Ministry of Education is gratefully acknowledged. Partial support from the Dirección General de Investigación Científica y Técnica (DGICYT, Madrid, Spain) through grant PB93-0955 is also greatly appreciated.

Accepted for publication 15 November 1995.

REFERENCES

1. Hart R. D. An introduction to distinct element modelling for rock engineering. General Report. *Proc. 7th Int. Congr. on Rock Mechanics* **3**, 1881–1891, Aachen (1991).
2. Alvarez A., Herrero E. and Buil J. M. Some considerations concerning the effect on overall safety of interface problems between arch dams and their foundations. *Treizième Congrès des Grands Barrages*, Q48, R67, 1169–1185, N. Delhi (1979).
3. Alvarez A., Herrero E. and Vizcaino M. Dams in karstified zones. Three different solutions. *Quinzième Congrès des Grands Barrages* C11, 1225–1246, Lausanne (1985).
4. Alvarez A., Herrero E. and Buil J. M. Strengthening of some exist dams. *Quinzième Congrès des Grands Barrages* Q59, R32, 505–526, Lausanne (1985).
5. Alonso E. E. and Carol I. Foundation analysis of an arch dam. Comparison of two modeling techniques: no tension and jointed rock material. *Rock Mech. Rock Engng* **18**, 149–182 (1985).
6. Carol I., Gens A. and Alonso E. E. A three-dimensional elasto-plastic joint element. *Int. Symp. Fundam. of Rock Joints* 441–451, Björkliden (1985).
7. Carol I., Gens A. and Alonso E. E. Three-dimensional model for rock joints. *Proc. 2nd Int. Conference on Numerical Models in Geomechanics* 179–189, Ghent (1986).
8. Gens A., Carol I. and Alonso E. E. An interface element formulation for the analysis of soil-reinforcement interaction. *Computers and Geotechnics* **7**, 133–151 (1988).
9. Zienkiewicz O. C. *The Finite Element Method in Engineering Science*. McGraw-Hill, London (1971).
10. Prat P., Gens A., Carol I., Ledesma A. and Gili J. A. DRAC: A computer software for the analysis of rock mechanics problems. *Proc. Int. Symp. on Application of Computer Methods in Rock Mechanics* **2**, 1361–1368, Xian (1993).
11. Bandis S., Lumsden A. C. and Barton N. R. Experimental studies of scale effects on the shear behaviour of rock joints. *Int. J. Rock Mech. Min. Sci & Geomech Abstr.* **18**, 1–21 (1981).

APPENDIX. EXPLICIT ELASTOPLASTIC JOINT CONSTITUTIVE MODEL

The basic variables adopted to formulate the model are the normal (σ) and shear-stresses (τ_1 and τ_2) on the joint, and the corresponding normal (u) and shear (v_1 and v_2) displacements (Fig. A1). The elastic behaviour is defined by:

$$\boldsymbol{\sigma}_j = \boldsymbol{D}^e \boldsymbol{\epsilon}_j \quad \boldsymbol{D}^e = \begin{pmatrix} K_n & 0 & 0 \\ 0 & K_t & 0 \\ 0 & 0 & K_t \end{pmatrix} \tag{A1}$$

where $\boldsymbol{\sigma}_j$ and $\boldsymbol{\epsilon}_j$ are the stress and strain vectors on joint j, and K_n and K_t are the normal and shear elastic stiffness, respectively, which are taken as constants.

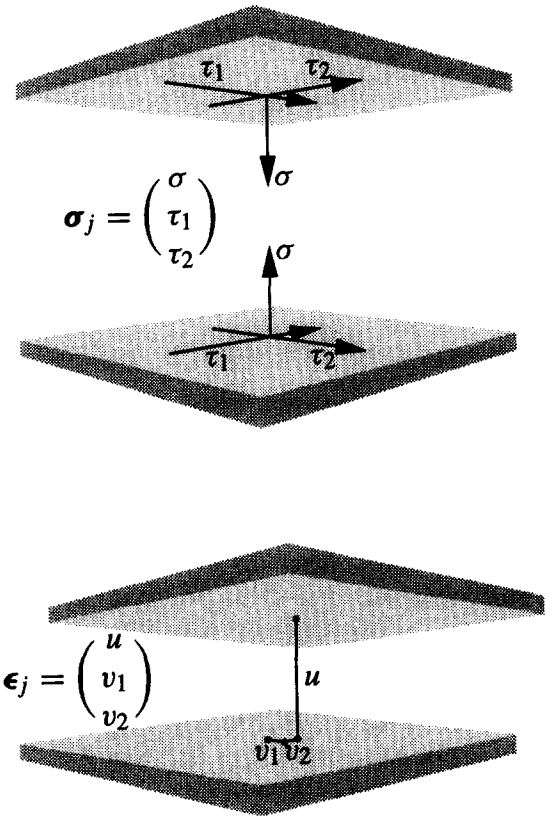

Fig. A1. Basic variables of the joint model.

The plastic model is defined by the following yield surface (Fig. A2):

$$F \equiv \tau_1^2 + \tau_2^2 - \tan^2\phi(\sigma^2 + 2a\sigma) = 0. \tag{A2}$$

Parameters a and $\tan\phi$ are the hardening parameters of the general hyperbolic model but remain constant in the simplified explicit model. This expression corresponds to a hyperbola passing through the origin in which $\tan\phi$ is the slope of the asymptote and $a = c/\tan\phi$ is the distance between the origin and the σ-axis intercept of the asymptote.

The integration problem can be stated as obtaining the new values of the stresses (σ, τ_1 and τ_2) given an arbitrarily imposed relative displacement increment (Δu, Δv_1 and Δv_2). The initial stress values are denoted as σ_0, $(\tau_1)_0$ and $(\tau_2)_0$. As shown in Fig. A3, the angle of the direction of the incremental relative displacement, Δv, with the Δv_1-axis is called β. Similarly, the angle of the tangential stress vector with the τ_1-axis is called θ.

The normal stress, σ, is related to u by the elastic relationship $\sigma = K_n u$ since dilatancy is assumed zero. The basic expressions for the incremental tangential stresses are

$$\begin{aligned} d\tau_1 &= K_t dv_1^e = K_t(dv_1 - dv_1^p) \\ d\tau_2 &= K_t dv_2^e = K_t(dv_2 - dv_2^p) \end{aligned} \tag{A3}$$

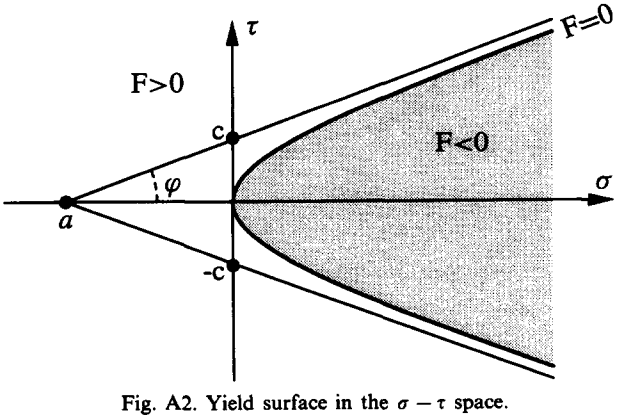

Fig. A2. Yield surface in the $\sigma - \tau$ space.

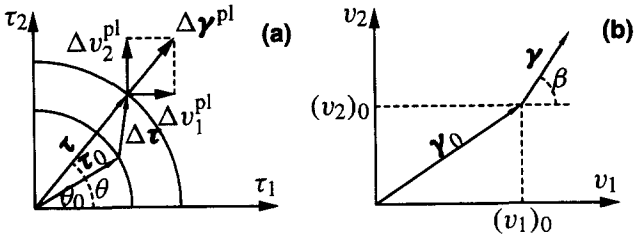

Fig. A3. (a) Yield surface in the $\tau_1 - \tau_2$ space; (b) variables in the strain space.

where dv_1, dv_2 are the total tangential relative displacement increments and dv_1^e, dv_2^e, dv_1^p and dv_2^p the elastic and plastic components.

Taking into account the flow rule in the τ_1–τ_2 plane, the plastic part of the tangential relative displacement increment can be written as

$$dv_1^p = dv^p \cos\theta$$
$$dv_2^p = dv^p \sin\theta. \tag{A4}$$

Also, the increments of τ_1 and τ_2 are related to the increments of τ and θ according to

$$d\tau_1 = d\tau\cos\theta - \tau\sin\theta\, d\theta$$
$$d\tau_2 = d\tau\sin\theta + \tau\cos\theta\, d\theta. \tag{A5}$$

From equations (A3–A5), the following differential equation is obtained:

$$\frac{K_t\, dv}{\tau} = \frac{d\theta}{\sin(\beta - \theta)}. \tag{A6}$$

This expression can be integrated because it is possible to reduce the left hand side to an expression with a single variable because dv is related to du as $dv = \Delta v/\Delta u\, du$, u is related to σ as indicated above and τ depends on σ according to the hyperbolic expression (A2).

Substituting these relations into equation (A6) and integrating, the equation

$$\tan\left(\frac{\beta - \theta}{2}\right) = \tan\left(\frac{\beta - \theta_0}{2}\right)\left[\frac{\tau + \sqrt{\tau^2 + a^2\tan^2\phi}}{\tau_0 + \sqrt{\tau_0^2 + a^2\tan^2\phi}}\right]^{\frac{-K_t\Delta v}{K_n\Delta u\tan\phi}} \tag{A7}$$

is obtained. From equation (A7) the new value of θ at the end of the relative displacement increment is computed.

Then, the complete new stress state can be determined since σ is obtained from u, τ is derived from equation (A6) and $\tau_1 = \tau\cos\theta$; $\tau_2 = \tau\sin\theta$. If desired, the plastic relative displacement increment can also be easily computed.